Supporting Information for

Stoichiometry Dependent Modifications in Synthetic Heme Peroxo Reactivity with Nitrosonium: A New Paradigm for Understanding Heme Mediated Nitration Chemistry

Samith B. Jayawardana,[a] Collin B. Gabel,[a] Arya A. Bhosale,[a] Aruzhan Abdikaiym,[a] Gbolagade Olajide,[b] Shanuk Rajapakse,[a] Tibor Szilvasi,*[,b] Brad S. Pierce,*[,a] Gayan B. Wijeratne*[,a]

[a] *Department of Chemistry and Biochemistry, University of Alabama, Tuscaloosa, Alabama 35401, United States.*

[b] *Department of Chemical and Biological Engineering, The University of Alabama, Tuscaloosa, Alabama, 35405, United States.*

*To whom correspondence should be addressed:
Gayan B. Wijeratne
gwijeratne@ua.edu

Experimental Section

1. Materials and Methods

All commercially available chemicals were purchased at the highest available purity and used as received unless otherwise stated. Air-sensitive compounds were handled either under an argon atmosphere using standard Schlenk techniques or in an MBRAUN Unilab Pro SP (<0.1 ppm of O2, <0.1 ppm of H2O) nitrogen-filled glovebox. All organic solvents were purchased at HPLC-grade or better. DCM and THF were degassed (by bubbling argon gas for 40 min at room temperature) and dried (by passing through a 60 cm alumina column) using an Inert Pure Solv MD 5 (2018) solvent purification system. These solvents were then stored in amber glass bottles inside the glovebox over 3 or 4 Å molecular sieves at least for 72 h prior to use. Benchtop UV-vis experiments were carried out using an Agilent Cary 60 spectrophotometer equipped with a liquid nitrogen-chilled Unisoku CoolSpek UV USP-203-B cryostat. A 2 mm path length quartz cell cuvette modified with an extended glass neck with a female 14/19 joint and stopcock was used to perform all UV-vis experiments. Low temperature ^{2}H NMR and ^{1}H NMR spectra were recorded on Bruker AV 360 MHz and Bruker DRX 400 MHz NMR spectrometers. All NMR spectra were recorded in 5 mm (outer diameter) tubes. The chemical shifts were re-ported as δ (ppm) values calibrated to natural abundance deuterium or proton solvent peaks. Electron paramagnetic resonance (EPR) spectra were collected in 4 mm (outer diameter) quartz tubes using an Xband Bruker EMX-plus spectrometer coupled to a Bruker ER 041 XG microwave bridge and a continuous-flow liquid helium cryostat (ESR900) controlled by an Oxford Instruments TC503 temperature controller (experimental conditions: microwave frequency = 9.41 GHz; microwave power = 0.2 mW; modulation frequency = 100 kHz; modulation amplitude = 10 G; temperature = 7 K). Nitrite was detected using a Molecular Probes Griess Reagent Kit (ThermoFisher G7921). 5,10,15,20-tetraphenylporphyrin iron (III) chloride, [H_2(TPP)],[1] 5,10,15,20-tetramesitylporphyrin, [H_2(TMP)],[2] 5,10,15,20-tetrakis(pentafluorophenyl)porphyrin, [H_2(F_{20}TPP)],[3] and [H_2(F_{20}TPP-d_8)][4] were synthesized by following published procedures. Metalation of the porphyrinates to generate [(TPP)Fe^{III}Cl], [(TMP)Fe^{III}Cl], [(F_{20}TPP)Fe^{III}Cl], and [(F_{20}TPP-d_8)Fe^{III}Cl] and the subsequent reduction to [$(THF)_2$(Por)Fe^{II}] (where Por = TPP, TMP, F_{20}TPP and F_{20}TPP-d_8) complexes were carried out by following previously published methods.[5] [(Por)Fe^{III}]SbF_6[6, 7] (where Por = TPP, TMP, F_{20}TPP and F_{20}TPP-d_8) complexes were synthesized following previously published literature procedures.

2. Formation of Heme Peroxide Adducts

The series of three electronically distinct heme peroxo adducts, [(F_{20}TPP)Fe^{III}(O_2^{2-})]$^-$ (F_{20}TPP (F_{20}TPP = 5,10,15,20-tetrakis(pentafluorophenyl)porphyrin)), [(TPP)Fe^{III}(O_2^{2-})]$^-$ (TPP (TPP = 5,10,15,20-tetraphenylporphyrin)), and [(TMP)Fe^{III}(O_2^{2-})]$^-$ (TMP (TMP = 5,10,15,20-tetramesitylporphyrin)) were prepared and characterized according to our previously published works.[8-10] F_{20}TPP was synthesized using a modified procedure employing chlorobenzene as solvent to replace dichloromethane.[3] Freshly distilled pyrrole (1.86 mL, 26.3 mmol), pentafluorobenzaldehyde (5.00 g, 25.0 mmol), and boron trifluoride diethyl etherate (300 µL, 2.43 mmol) were dissolved in chlorobenzene (400 mL) and stirred under argon atmosphere at 50 °C for 44 h. 2,3-dichloro-5,6-dicyano-1,4-benzoquinone (DDQ, 5.8 g, 25.04 mmol) was then added, and the reaction mixture was stirred for an additional 1.5 h. The solvent was removed under reduced pressure, and the crude product was dissolved in chloroform:hexane (1:1) and filtered through silica. The filtrate was concentrated to form a slurry and further purified by flash column

chromatography using a gradient elution starting with pure hexane and progressing to hexane:chloroform (4:1). Violet crystals were obtained (1.2 g, 19.4% yield). In that, the ferrous heme complex, $[(THF)_2(F_{20}TPP)Fe^{II}]$, exhibited significant electronic absorption changes from 420 (Soret; $\varepsilon = 3.4\times10^5$ $M^{-1}cm^{-1}$) and 540 nm ($\varepsilon = 1.7\times10^4$ $M^{-1}cm^{-1}$) to 413 (Soret; $\varepsilon = 1.9\times10^5$ $M^{-1}cm^{-1}$) and 535 ($\varepsilon = 1.8\times10^4$ $M^{-1}cm^{-1}$) nm in 9:1 DCM:THF solvent mixture upon the bubbling of dry $O_{2(g)}$ (Fig S1A) at −80 °C. These changes are characteristic of the formation of EPR-silent, end-on ferric superoxo species, $[(F_{20}TPP)Fe^{III}(O_2^{-\bullet})]$, as previously reported by us and others. Subsequent addition of 1 equiv of cobaltocene reductant led to the formation of the side-on ferric peroxo species, $[(F_{20}TPP)Fe^{III}(O_2^{2-})]^-$, with electronic absorption features centered at 432 (Soret; $\varepsilon = 3.0\times10^5$ $M^{-1}cm^{-1}$) and 557 ($\varepsilon = 2.1\times10^4$ $M^{-1}cm^{-1}$) nm (Fig S1A). This heme peroxo complex indicated an EPR feature at g = 4.2 demonstrating the presence of a rhombic high-spin Fe^{III} center.[11] Furthermore, these transformations were also followed by low-temperature ^2H NMR spectroscopy using the pyrrole-position deuterated $F_{20}TPP{-}d_8$ porphyrinate, wherein $[(THF)_2(F_{20}TPP{-}d_8)Fe^{II}]$ exhibited a single ^2H NMR feature at $\delta_{pyrrole}$ = 93.0 ppm, which moved up-field to $\delta_{pyrrole}$= 9.3 ppm upon the formation of $[(F_{20}TPP{-}d_8)Fe^{III}(O_2^{-\bullet})]$. Formation of the corresponding heme peroxo species, $[(F_{20}TPP{-}d_8)Fe^{III}(O_2^{2-})]^-$, moved this feature down to $\delta_{pyrrole}$ = 95.8 ppm (Fig S1C). These characterization data are in good agreement with those reported previously. Analogous changes in UV-vis and EPR spectroscopic signatures characteristic of the aforementioned formation of $[(Por)Fe^{III}(O_2^{-\bullet})]$ and $[(Por)Fe^{III}(O_2^{2-})]^-$ from the corresponding ferrous complexes were also observed for the TPP and TMP systems (Fig S2).[12]

3. Low temperature ^2H NMR spectroscopic studies

For a typical ^2H NMR experiment, $[(F_{20}TPP\text{-}d_8)Fe^{II}]$ (10 mg, 0.01 mmol) was dissolved in 0.5 mL of 9:1 DCM:THF in a 5 mm (outer diameter) NMR tube inside the glovebox and was sealed with a rubber septum. This tube was then stabilized at −80 °C using a liquid nitrogen/acetone cold bath. Then dry $O_{2(g)}$ was bubbled through the solution using a three-way gastight syringe to generate the corresponding superoxide complex, $[(F_{20}TPP\text{-}d_8)Fe^{III}(O_2^{-\bullet})]$. Subsequently, 1 equiv of cobaltocene was added in to generate the corresponding $[(F_{20}TPP\text{-}d_8)Fe^{III}(O_2^{2-})]^-$ complex. 4 equiv of $NOPF_6$ (in MeCN) was added separately into $[(F_{20}TPP\text{-}d_8)Fe^{III}(O_2^{2-})]^-$ complex. For each instance, the NMR tube was immediately transferred into the NMR cryostat held at −80 °C for data accumulation (Fig 2A and S10).

4. EPR spectroscopic studies

Sample preparation for EPR experiments were carried out as follows: 150 μL of the heme complex, $[(F_{20}TPP)Fe^{II}]$ (in 9:1 DCM:THF; 2 mM) was placed in a 250 mm EPR tube (4 mm O.D.) and was sealed with a rubber septum inside the glovebox. Following cooling down to −80 °C (using liquid nitrogen/acetone cold bath), then dry $O_{2(g)}$ was bubbled through the solution using a three-way gastight syringe to generate the corresponding superoxide complex, $[(F_{20}TPP\text{-}d_8)Fe^{III}(O_2^{-\bullet})]$, under inert conditions and excess $O_{2(g)}$ was removed by purging Ar. 1 equiv of cobaltocene was added in to form $[(F_{20}TPP)Fe^{III}(O_2^{2-})]^-$ complex, then 4 equivalent of $NOPF_6$ (in MeCN) was added separately into $[(F_{20}TPP)Fe^{III}(O_2^{2-})]^-$ complex. For each instance, the EPR tube was immediately frozen in liquid nitrogen, and was transferred into the cryostat of an EPR spectrometer.

5. Nitration of 2,4-di-tert-butylphenol (2, 4-DTBP)

Immediately after the addition of 4 equiv of $NOPF_6$ (in MeCN) into $[(F_{20}TPP)Fe^{III}(O_2^{2-})]^-$ (0.049 mmol) in 9:1 DCM:THF (10 mL), 2, 4-di-*tert*-butylphenol (2,4-DTBP; 202 mg, 0.98 mmol in 100 μL of DCM) was added quickly using a gastight syringe and the solution was stirred at −80 °C for 20 min before warming up to room temperature. The final reaction mixture was dried in vacuum and the major organic product (2,4-di-*tert*-butyl-6-nitrophenol) was purified by silica gel column chromatography using hexane: EtOAc = 9:1 as the eluent; it was characterized by ^{1}H NMR (Fig S7), GC-MS (Fig S15A), and the other 3,3',5,5'-tetra-*tert*-butylbiphenyl-2,2'-diol product was characterized by GC-MS.

To probe the mechanism of $^{\bullet}NO_2$ generation and subsequent reactivity, we performed quantitative product analysis and isotope labeling experiments. A solution of $[(F_{20}TPP)Fe^{III}(O_2^{2-})]^-$ or $[(F_{20}TPP)Fe^{III}(^{18}O_2^{2-})]^-$ (0.008 mmol) in 9:1 DCM:THF (1 mL) was treated with 4 equiv of $NOPF_6$ (or $^{15}NOBF_4$ for nitrogen labeling) in MeCN at –80 °C. 20 equiv of 2,4-DTBP in DCM was added rapidly via gastight syringe and the reaction mixture was maintained at –80 °C for 20 min to ensure complete reaction, then warmed to room temperature. Products were analyzed by GC-MS for structural characterization and quantification (Fig S15).

To confirm that the heme-peroxo complex is essential for nitrophenol formation, a control reaction was performed under identical conditions but in the absence of iron porphyrin. A solution containing only 9:1 DCM:THF (1 mL) was cooled to –80 °C, treated with $O_{2(g)}$, Ar degassing, 1 equiv of cobaltocene and 4 equiv of $NOPF_6$ in MeCN respectively (based on the molar amount used in heme experiments), followed by rapid addition of 20 equiv of 2,4-DTBP. After maintaining at –80 °C for 20 min and warming to room temperature, GC-MS analysis revealed no detectable nitrophenol or bisphenol coupling products (Fig S13).

Parallel experiments with alternative substrates were conducted following identical procedures: 3-methylindole and 5,6-O-isopropylidene-L-ascorbic acid (10 equiv) utilized in place of 2,4-DTBP as mentioned above, and final product were characterized by ESI-MS (Fig S16 and S17).

6. Semi-quantitative analysis of nitrate and nitrite anions in the final reaction product

The final reaction mixtures between $[(F_{20}TPP)Fe^{III}(O_2^{2-})]^-$ and 4 equiv of $NOPF_6$ were warmed up to room temperature (vide supra), and the solvent was removed under vacuum. The resulting solid was then redissolved in 10 mL DCM and extracted with 20 mL of aqueous NaCl solution (6 mM). Approximate stoichiometric yields of nitrite and nitrate anions, in addition of 4 equiv of $NOPF_6$ reaction sample, in aqueous layer were calculated using semiquantitative QUANTOFIX nitrite test strips.[13]

7. Quantitative analysis by Griess assay analysis for nitrate and nitrite anions in the final reaction product

In the glovebox a 25 mL Schlenk Flask equipped with stir bar was containing $[(F_{20}TPP)Fe^{II}]$ (10 mg, 0.01 mmol) in 9:1 DCM:THF (5 mL), and was sealed with a rubber septum. The flask was cooled in a liquid N_2/acetone bath adjusted to −80 °C. Then dry $O_{2(g)}$ was bubbled through the solution using a three-way gastight syringe to generate the corresponding superoxide complex, $[(F_{20}TPP)Fe^{III}(O_2^{-\bullet})]$, under inert conditions and excess $O_{2(g)}$ was removed by purging Ar. 1 equiv of cobaltocene was added in to form $[(F_{20}TPP)Fe^{III}(O_2^{2-})]^-$ complex. Then 4 equiv of $NOPF_6$ (in

MeCN) was added. The reaction was allowed to run 10 min and allowed to warm up to room. The solvent was then removed and the resulting solid redissolved in 3 mL of dichloromethane. The dichloromethane solution was extracted three times with 3, 3, and 4 mL of $NaCl_{(aq)}$ (20 mM). The combined aqueous phases were tested for nitrite via the Griess Assay (Molecular Probes Griess Reagent Kit; ThermoFisher G7921). Modified Griess Assay test was performed to quantify the nitrate yield by previously published.[14-16]

8. In situ generation of authentic [(F_{20}TPP-d_8)$Fe^{III}(NO_2)_2$] complex

[(F_{20}TPP-d_8)$Fe^{III}(NO_2)$] was generated by bubbling 2 mL of $NO_{2(g)}$ to a 9:1 DCM:THF solution (0.5 mL) of [(F_{20}TPP-d_8)Fe^{III}]SbF_6 (10 mg, 0.001 mmol) complex at –80 °C (Fig S10).

9. N_2O Quantification

Bulk reactions were carried out by a 20 mL Agilent headspace vial, equipped with a magnetic stir bar, containing [(F_{20}TPP)Fe^{II}] (8.175 mg, 0.008 mmol) in 9:1 DCM:THF (1 mL), inside the glovebox and was sealed with a headspace cap. The vial was cooled in a liquid N_2/ acetone bath adjusted to −80 °C. Then dry $O_{2(g)}$ was bubbled through the solution using a three-way gastight syringe to generate the corresponding superoxide complex, [(F_{20}TPP)$Fe^{III}(O_2^{-\bullet})$], under inert conditions and excess $O_{2(g)}$ was removed by purging Ar. 1 equiv of cobaltocene was added in to form [(F_{20}TPP)$Fe^{III}(O_2^{2-})]^-$ complex. 20 equiv of 2,4-DTBP (in DCM) was added followed by addition of 4 equiv of $NOPF_6$ (in MeCN). The reaction mixture was stirred for 5 minutes at −80 °C, then warmed to room temperature. Headspace N_2O was quantified by GC-ECD using N_2O standards prepared according to literature procedure (Fig S12).[17]

10. Computational Methods

All density functional theory (DFT) calculations were performed using the Gaussian 16 software package.[18] Geometry optimizations and single-point energy calculations were conducted at the UB3LYP-D3BJ(SMD=DCM)/def2-TZVP//UB3LYP-D3BJ(SMD=DCM)/def2-SVP level of theory,[19-24] The application of implicit solvation to reactive cationic species such as NO^+ may introduce uncertainties, but this approach is not anticipated to affect the qualitative trends reported herein. All physically meaningful spin states were tested up to multiplicity of 6 for all stationary points and confirm each by normal-mode analysis. Experimental reaction conditions were applied using GoodVibes program,[25] and corrected all computed energetics from a gas-phase standard state to the experimental reaction temperature of 193.15 K. Optimized Cartesian coordinates for all calculated structures are provided below.

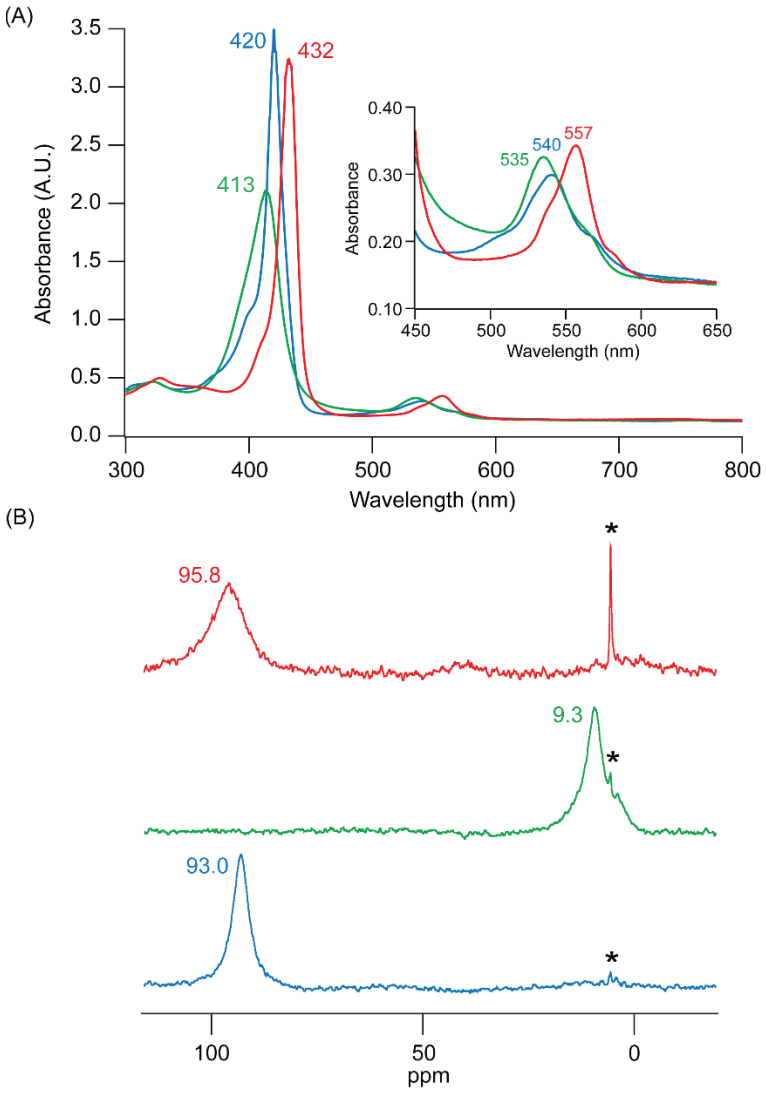

Fig. S1 (A) UV−vis spectral changes in 9:1 DCM:THF at −80 °C of 50 μM [$(THF)_2(F_{20}TPP)Fe^{II}$] (blue), [$(F_{20}TPP)Fe^{III}(O_2^{\bullet-})$] (green), and [$(F_{20}TPP)Fe^{III}(O_2^{2-})]^-$ (red). (B) ^2H NMR spectral data in 9:1 DCM:THF for [$(THF)_2(F_{20}TPP{-}d_8)Fe^{II}$] (blue), [$(F_{20}TPP{-}d_8)Fe^{III}(O_2^{\bullet-})$] (green), and [$(F_{20}TPP{-}d_8)Fe^{III}(O_2^{2-})]^-$ (red).[12]

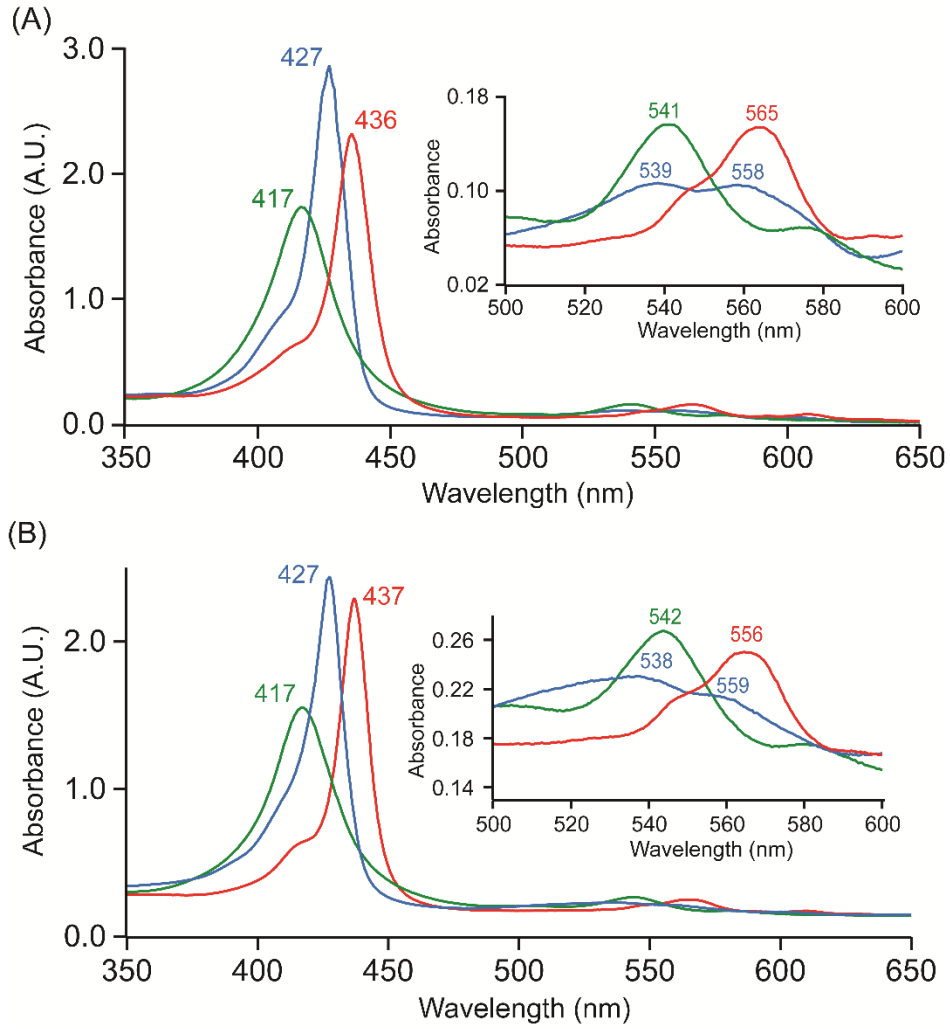

Fig. S2 UV−vis spectral changes in 9:1 DCM:THF at −80 °C of 50 μM (A) $[(THF)_2(TPP)Fe^{II}]$ (blue), $[(TPP)Fe^{III}(O_2^{-\bullet})]$ (green), $[(TPP)Fe^{III}(O_2^{2-})]^-$ (red) and (B) $[(THF)_2(TMP)Fe^{II}]$ (blue), $[(TMP)Fe^{III}(O_2^{-\bullet})]$ (green), $[(TMP)Fe^{III}(O_2^{2-})]^-$ (red). Insets show the expanded Q-band regions.[12]

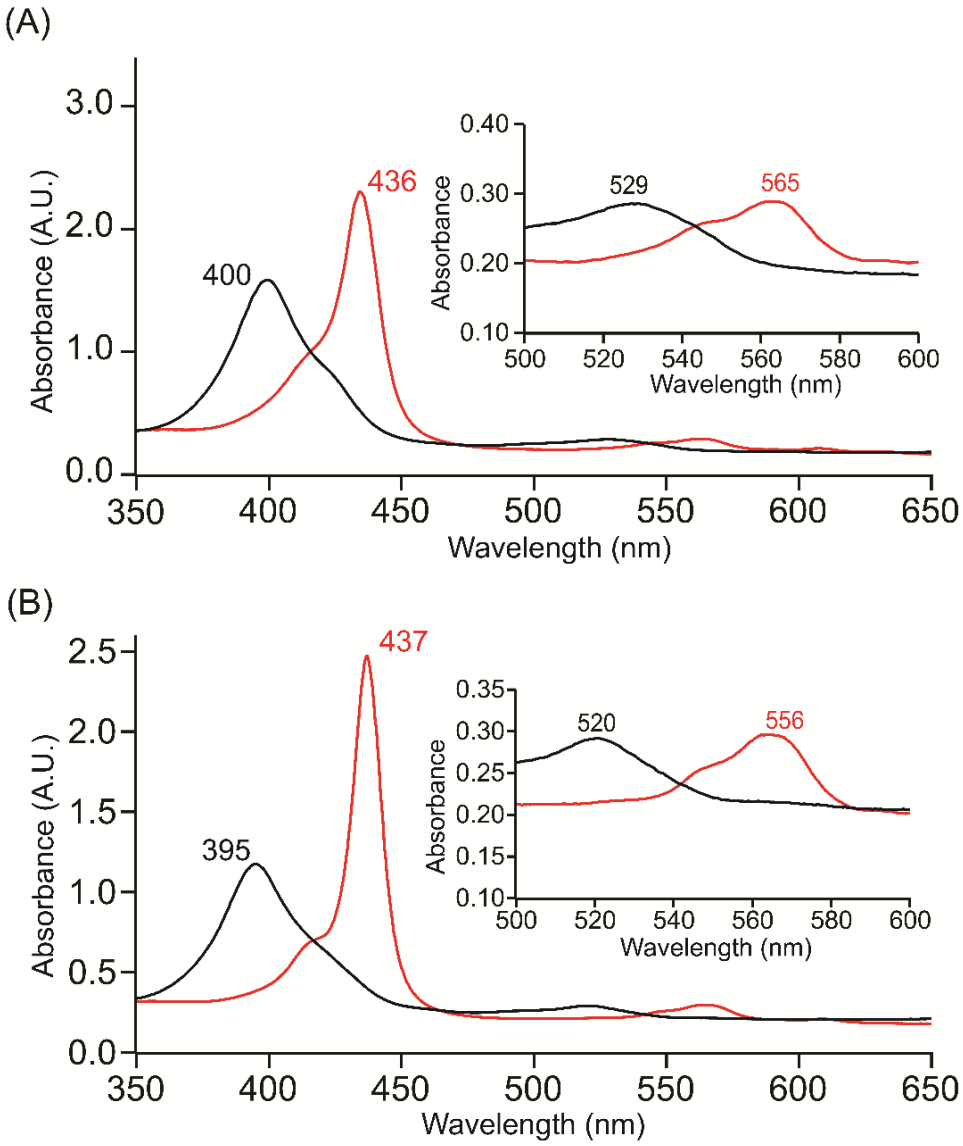

Fig. S3 UV−vis spectral changes in 9:1 DCM:THF at −80 °C of $[(Por)Fe^{III}(O_2^{2-})]^-$ (red) and after addition of 4 equiv $NOPF_6$ (black). Por = (A) TPP (B) TMP. Insets show the expanded Q-band regions.

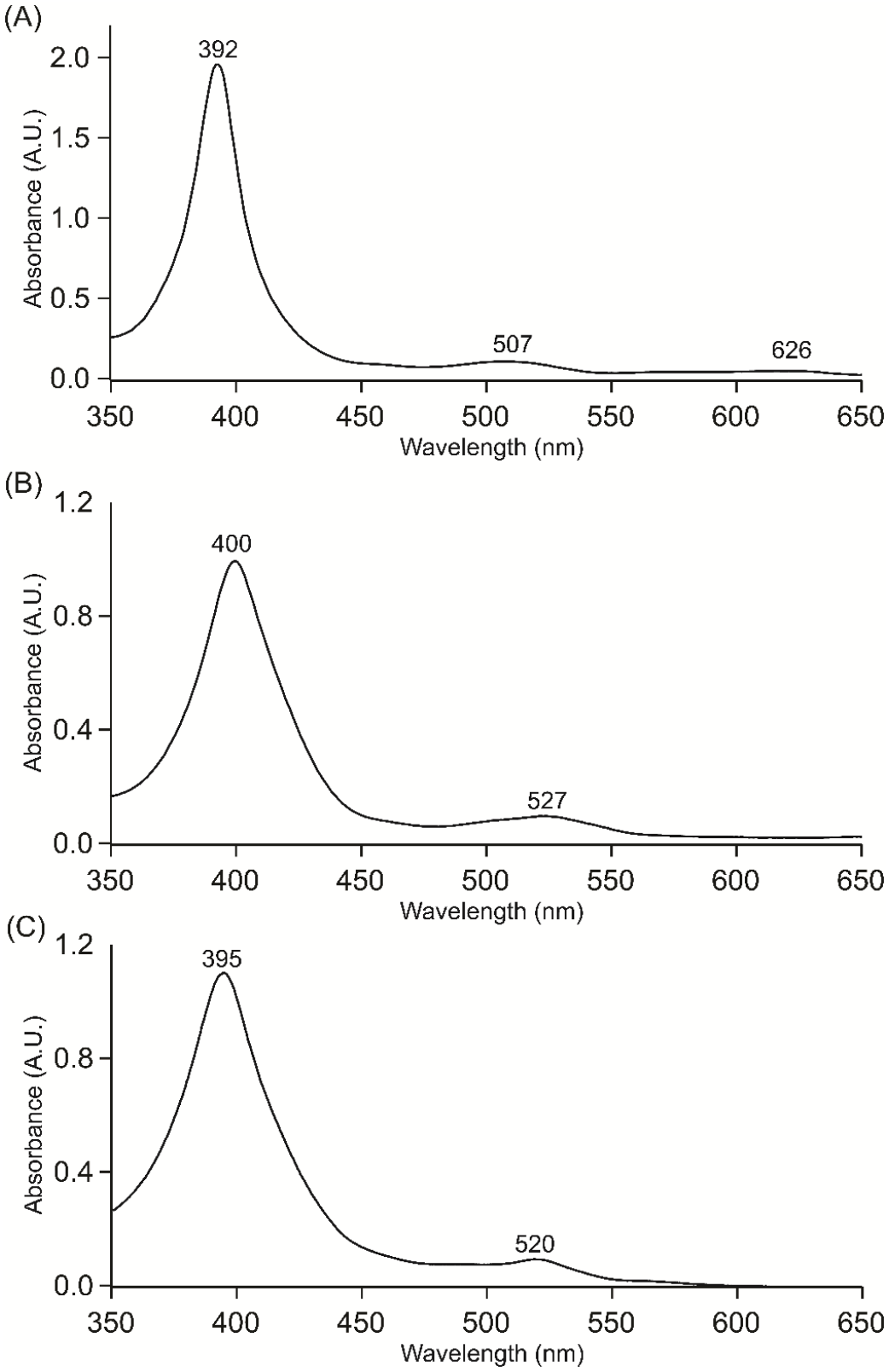

Fig. S4 (i) UV−vis spectra in 9:1 DCM:THF at 25 °C for [(Por)$Fe^{III}(SbF_6)$]. Por = (A) F_{20}TPP (B) TPP (C) TMP.

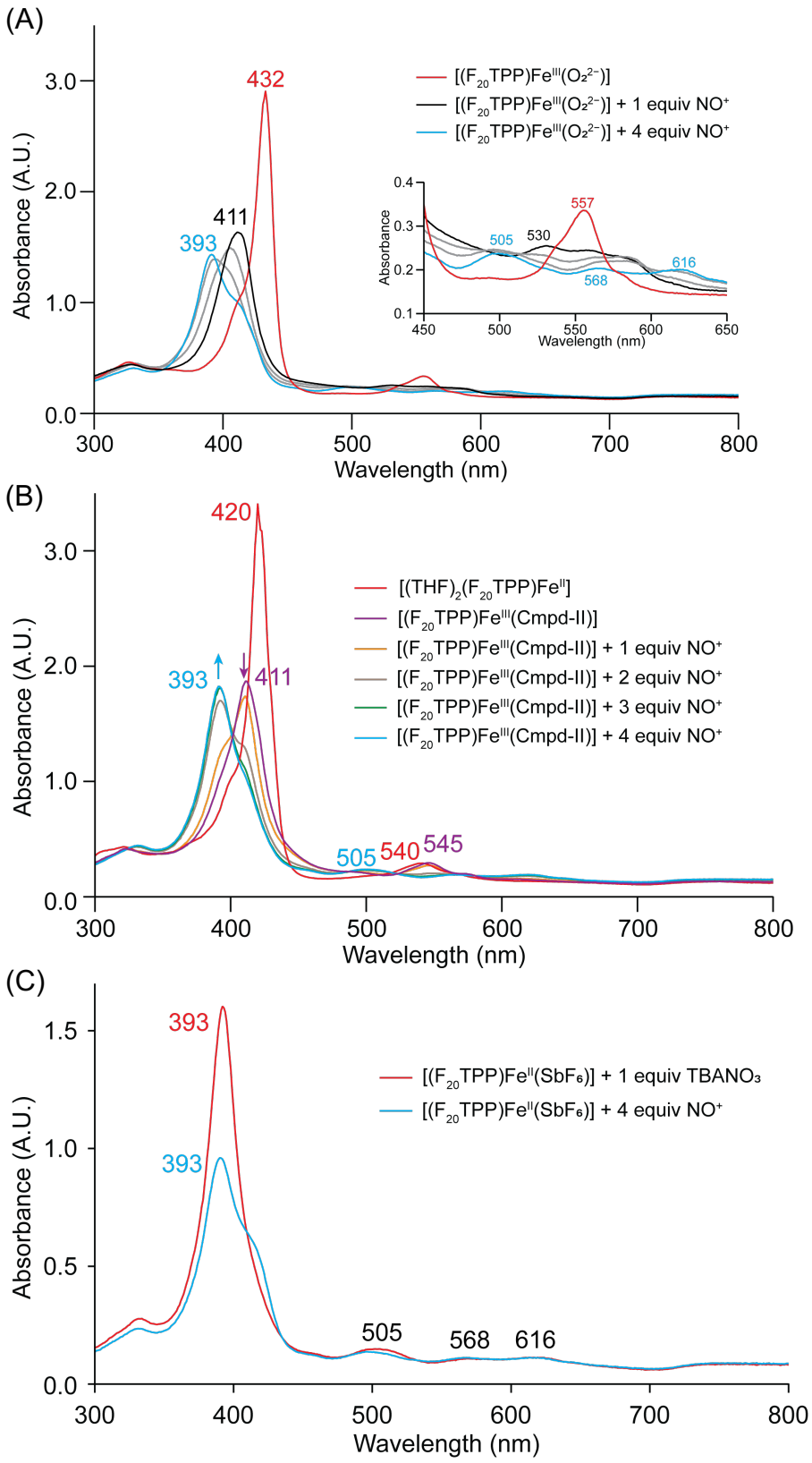

Fig. S4 (ii) UV−vis spectra in 9:1 DCM:THF at -80 °C indicating the reactivity of (A) [(F_{20}TPP)Fe^{III}(OONO)] (black), (B) [(F_{20}TPP)Fe^{IV}(O)], and (C) [(F_{20}TPP)Fe^{III}](NO_3) with NO^+.

EPR simulations. EPR simulations were calculated using SpinCount developed by Professor Michael Hendrich at Carnegie Mellon University by utilizing the general spin Hamiltonian as shown in equation **S1**.[26-28]

$$\widehat{H} = \boldsymbol{D}\left(\hat{S}_Z^2 - \frac{\hat{S}^2}{3}\right) + \boldsymbol{E}\left(\hat{S}_X^2 - \hat{S}_Y^2\right) + \beta_e \boldsymbol{S} \cdot \widetilde{\boldsymbol{g}} \cdot \mathbf{B} + \mathbf{S} \cdot \widetilde{\mathbf{A}} \cdot \mathbf{I} \qquad \textbf{equation S1}$$

Here, $\widetilde{\boldsymbol{g}}$ and $\widetilde{\boldsymbol{A}}$ represent the intrinsic *g*- and *A*-tensors for the paramagnetic center with spin ($\boldsymbol{S}$). Hyperfine splitting is treated by second-order perturbation theory.[29,30] Axial and rhombic zero-field splitting (*zfs*) terms are represented by $\boldsymbol{D}$ and $\boldsymbol{E}$, respectively. This program computes the powder pattern for a uniform spherical distribution of the magnetic field vector $\boldsymbol{B}$, and the transition intensities are calculated using '*Fermi's golden rule*'.[31] All simulations were generated with consideration of all intensity factors, both theoretical and experimental, to allow for determination of species concentration. The only unknown factor relating spin concentration to signal intensity was an instrumental factor that is specific to the microwave detection system. However, this was determined by the spin standard, 1.0 mM aqueous Cu(EDTA) with 20% (v/v) glycerol, prepared from a copper atomic absorption standard solution purchased from Sigma-Aldrich.

The energy separating the ground doublet from excited states for an S = 5/2 spin center was obtained experimentally by fitting the temperature-normalized signal area (S×T) for data collected across a broad temperature range (4 - 50 K) to a Boltzmann population distribution for a 3-level system (**equation S2**).

$$\boldsymbol{S \times T \sim n_s} = \frac{\boldsymbol{g_i \cdot e^{-\Delta E_i / k_b T}}}{\sum_j \boldsymbol{g_j \cdot e^{-\Delta E_j / k_b T}}} = \frac{\boldsymbol{(2S_i + 1) \cdot e^{-D S_{z,i}^2 / k_b T}}}{\sum_j \boldsymbol{(2S_j + 1) \cdot e^{-D S_{z,j}^2 / k_b T}}} \qquad \textbf{equation S2}$$

Analysis of observed EPR spectra. **Figure S1** presents the EPR spectra for samples taken at representative points in the reaction of treatment of $[(F_{20}TPP)Fe^{III}(O_2^{2-})]^-$ with 4 equiv $NOPF_6$. The η^2-peroxo complex of $F_{20}TPP\text{-}Fe^{III}$ is shown in trace [**1**]. The signal observed at $g \sim 4.2$ originates from the middle doublets of a rhombic (E/D = 0.25) high-spin (S =5/2) ferric iron. A full description of the temperature dependent EPR characterization and analytical simulation of this species is presented elsewhere.[32] Spectrum [**2**] was observed for samples collected immediately following treatment of $[(F_{20}TPP)Fe^{III}(O_2^{2-})]^-$ with 4 equiv. $NOPF_6$ in 9:1 DCM:THF at -80 °C. The observed *g*-values (6.03, 5.97, and 2.00) indicate that this signal originates from a transition within the |±1/2> doublet of a S = 5/2 paramagnetic center with near axial symmetry (E/D = 0.001). As shown in **Figure S2B** (□), the temperature normalized signal area (**S×T**) decreases with increasing temperature demonstrating the this is the ground doublet (D > 0). A quantitative simulation (**Sim1**) of this species is overlaid on the spectrum [**2**] for comparison.

Samples were then warmed up to room temperature and re-frozen to observe the EPR spectra for the final, thermodynamic product (shown in trace [**3**]). As before, a nearly axial heme is observed (E/D = 0.001) with similar *g*-values to those observed in trace [**2**]. However, in addition to this species, a second high-spin signal can be identified by the $g \sim 6.35$ 'shoulder' (*) (**Figure S1**, trace [**3**]). This signal is attributed to a more rhombic heme ($E/D \sim 0.015$) species. For clarity, the axial heme signal was subtracted from spectrum [**3**]. The resulting difference spectra (trace [**3'**]**)** shows

the isolated signal from the more rhombic heme (scaled by 3-fold). A simulation (**Sim2**) of this species is overlaid on the difference spectra. For comparison, the EPR spectrum for the authentic $F_{20}TPPFe^{III}$-complex is shown in trace. While the decreased intensity of this signal may suggest a lower concentration relative to the axial heme, this is incorrect as the anisotropy of this signal vastly decreases the apparent intensity. Therefore, analytical quantitation of this signal was performed by spectroscopic simulation using the experimentally determined *D*-value (discussed below. From this analysis, we conclude that the more rhombic heme species (*E*/*D* = 0.015) is the major product, representing 86% of the observed high-spin heme signal. The remaining 36% can be attributed to the near axial heme. For comparison, the EPR spectrum for the samples of the authentic $F_{20}TPPFe^{III}$-complex is shown in trace [**4**]. Once again, a near axial high-spin ferric heme is observed with nearly equivalent *g*-values as those observed for the near axial heme present in [**2**] and [**3**]. As observed in **Figure S3A**, a minor shift in *g*-values and line width is observed by comparing spectrum [**4**] relative to [**2**]. Since both *g*-values and rhombicity (*E*/*D*) are nearly equivalent, differentiation of these species requires temperature dependent analysis of signal intensity to evaluate the axial zero field splitting term (*D*-value) for each species.

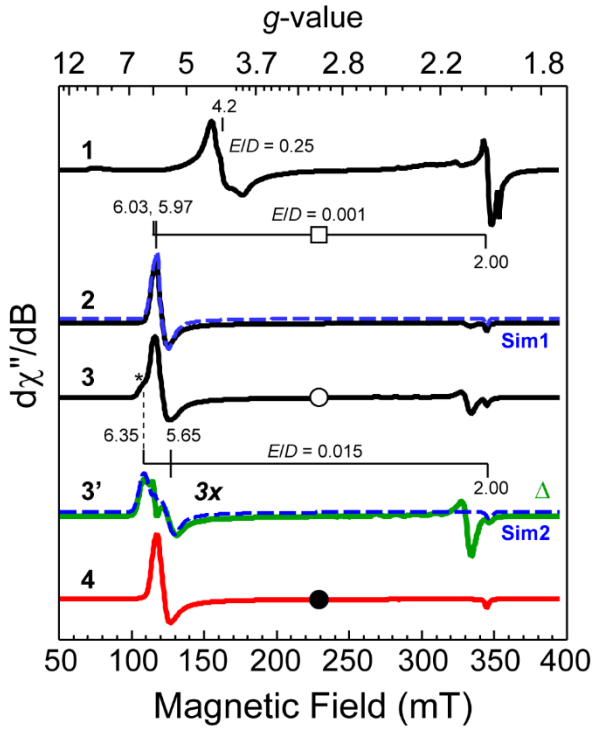

Fig. S5 Representative X-band CW EPR spectra illustrating the observed species upon treatment of $[(F_{20}TPP)Fe^{III}(O_2^{2-})]^-$ with 4 equiv $NOPF_6$. Trace [**1**] shows the EPR spectra for the η^2-Fe^{III}-peroxo complex observed before addition of nitrosonium ion. The high-spin axial signal observed immediately following addition of 4 equiv. $NOPF_6$.is shown in trace [**2**]. This signal can be simulated (**Sim1**, *dashed blue line*) assuming a minor shift from axial symmetry (*E*/*D* = 0.001). Spectrum [**3**] represents the observed EPR spectra of the final heme product after warming samples of [**2**] to room temperature. The '*shoulder*' observed at *g* ~ 6.35 (*) can be attributed to a contribution from a rhombically distorted high-spin heme (*E*/*D* = 0.015). Trace [**3'**] shows the isolated rhombic heme (scaled by 3-fold) following subtraction of the axial heme. A simulation

(**Sim2**) of this species is overlaid on the difference spectra. For comparison, the EPR spectrum for the authentic $F_{20}TPPFe^{III}$-complex is shown in trace [**4**]. Simulation parameters for **Sim1** and **Sim2** are summarized in **Table S1**. *Instrumental parameters*: microwave frequency, 9.63 GHz, microwave power, 21 mW (**1**), 0.7 mW [**2**] - [**4**]; temperature, 7 K; modulation amplitude, 0.9 mT.

Temperature dependence of EPR data. For a d^5 ion, the magnitude of zero field splitting parameters E and D are dependent on the extent of orbital mixing between the ground $^6A_1$ state and the lowest lying excited states. Under tetragonal distortion (**Figure S2**), the energy separating the ground and lowest lying $^4A_2$ and ^4E states are represented by Δ_1 and Δ_2, respectively. As the systems being considered have near axial g-values (6, 6, and 2), the influence of rhombic distortion is neglected ($E \sim 0$). Withing this regime, the magnitude of the axial zero field splitting parameter (D-value) is described by equation **S3**. In this expression, λ represents the spin-orbit coupling constant for Fe^{III} [340 cm^{-1}] and the D-value is positive providing $\Delta_2 > \Delta_1$.[33-35] While the D-value is sensitive to ligand environment and geometry, it should be noted that its numerical value is context dependent and thus cannot be used by itself to establish the binding of a specific ligand or coordination number. That being said, it is reasonable to assume that a decrease in D-value likely represents an increase in coordination number among equivalent heme complexes.

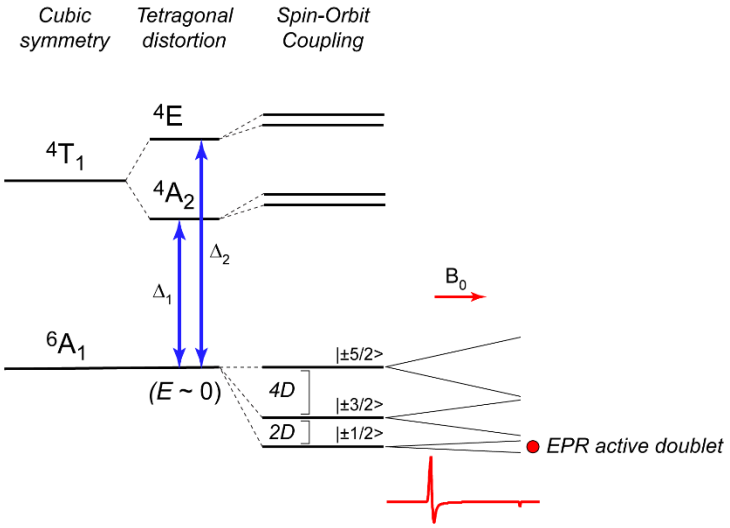

Fig. S6 Crystal field splitting diagram for high-spin d^5 ion under axial distortion.

$$D = \frac{\lambda^2}{5}\left[\frac{1}{\Delta_1} - \frac{1}{\Delta_2}\right] \qquad \textbf{equation S3}$$

Since the nature and number of coordinating ligands influences Δ_1 and Δ_2, the D-value provides an additional metric to differentiate interrogate the heme coordination environment even when g- and E/D-values are overlapping.

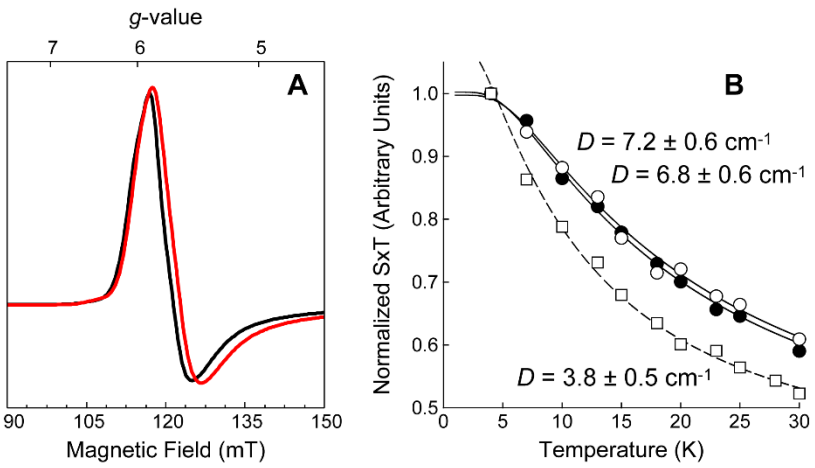

Fig. S7 Panel **A** shows an expansion of the $g_{\perp}$-region for overlaid spectra [**2**] and [**4**] for ease of comparison. Panel **B** provides the temperature normalized signal area (S×T) measured for samples [**2**] (□), [**3**] (○), and [**4**] (●). The *D*-values shown were obtained by fitting the data (*overlaid solid and dashed lines*) to a Boltzmann population distribution for a 3-level system (equation **S2**).

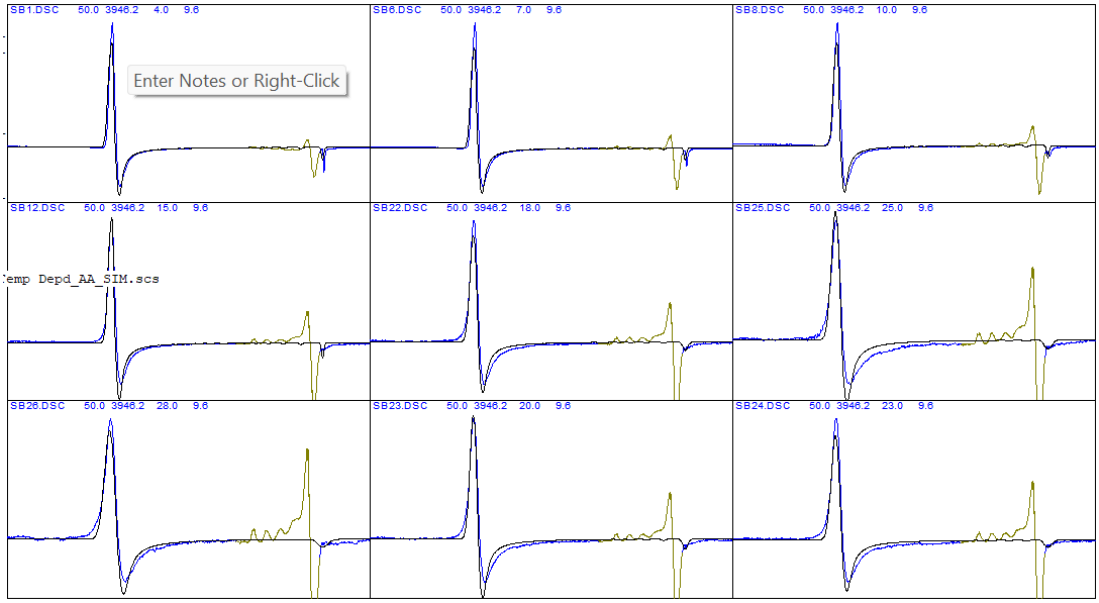

Fig. S8. Screenshot of SpinCount simulation of sample [**2**] treated with excess nitrosonium ion (NO^+). at selected temperatures (T = 4, 7, 10, 15, 18, 20, 23, 25, and 28 30 K). Simulations parameters are provided in **Table S1**.

To determine the *D*-value, EPR spectra were recorded at multiple temperatures (n = 10) and microwave power settings spanning 4 to 30 K. The signal area was then determined for each spectrum by double integration, then multiplied by its corresponding temperature (**S**×**T**). This value was plotted as a function of temperature and fit to a Boltzmann population curve for a 3-

level system according to equation **S2**. **Figure S3B** compares the non-Curie law temperature dependent behavior observed for samples [**2**] (□), [**3**] (○), and [**4**] (●). Significantly, the temperature normalized signal intensity of [**3**] (7.2 ± 0.5 cm^{-1}) and [**4**] (6.8 ± 0.5 cm^{-1}) are equivalent. However, sample [**2**] (3.8 ± 0.6 cm^{-1}) exhibits a *D*-value nearly half the magnitude of [**3**] and [**4**].

Additional corroboration of the above *D*-values was obtained by SpinCount. Here, the relative intensity of signals observed in [**2**], [**3**], and [**4**] were simultaneously simulated for nine different temperatures spanning 4 to 30 K. As shown in the screenshot (**Figure S3**) the relative intensity of high-spin signal is faithfully reproduced using the experimentally determined *D*-value [3.8 cm^{-1}]. A similar validation was performed for samples [**3**] and [**4**]. For comparison, *D*-values reported for biological heme system range between 4 and 12 cm^{-1}.[34, 36, 37]

Despite the overlap in observed *g*-values and rhombicity (*E*/*D*), temperature dependent EPR studies reveal a ~2-fold decrease in *D*-value for the near axial heme observed in trace [**2**] relative to the authentic $F_{20}TPPFe^{III}$-complex (trance [**4**]). As both signals exhibit near zero rhombicity, equation **S3** can be used to infer that the tetragonal distortion (separation between Δ_2 and Δ_1) is larger for $F_{20}TPPFe^{III}$-complex. Since the authentic standard is four-coordinate, the simplest explanation for the two-fold decrease in *D*-value observed for sample [**2**] is that this species has a higher coordination number; thereby shifting the symmetry of the complex toward octahedral symmetry.

The nature of hemes observed upon warming to room temperature is more complicated due to the mixture of species observed. The matching *D*-value for the near axial heme [7.2 ± 0.5 cm^{-1}] in trace [**3**] suggest that a four-coordinate heme, equivalent to the authentic $F_{20}TPPFe^{III}$-complex is one final product of this reaction. However, the second, more rhombic ([**3'**], *E*/*D* = 0.015) heme represents the majority product. Of note, the *g* ~ 6.35 (*) '*shoulder*' is obscured at temperatures above 15 K due to line broadening. Consequently, a narrow range of temperatures (4, 7, 13, and 15 K) was used to establish a lower limit *D*-value magnitude [~10 cm^{-1}].

Table S1. *EPR spectroscopic parameters for species observed following treatment of* $[F_{20}TPP)Fe^{III}(O_2^{2-})]^-$ *with 4 equiv. nitrosonium* (NO^+).

Sample	Spin	*Observed g-values**	*D* (cm^{-1})	*E*/*D*
1	5/2	4.2	0.7 ± 0.1	0.25
2	5/2	6.0, 6.0, 2.0	3.8 ± 0.5	0.001
3	5/2	6.0, 6.0, 2.0	7.2 ± 0.6	0.001
3'	5/2	6.6, 5.4, 2.0	~10	0.015
4	5/2	6.0, 6.0, 2.0	6.8 ± 0.6	0.001

***** EPR simulations for all high-spin ($S = 5/2$) ferric sites use isotropic ($g_{x,y,z} = 2.0$) intrinsic *g*-values which are typical for a Fe(III) d^5-ion. Simulated linewidths (σ_B) for spectra were fixed at the instrumental modulation amplitude (0.9 mT) used for all data collection.

Identification of N-centered radical and Cu(II) impurity. In samples treated with 4 mol equiv. NO^+ [**2**], a sharp isotropic signal at g ~2.008 (▼) with triplet hyperfine splitting is observed if analyzed within 1 hour of preparation. The equal intensity of each hyperfine transition (1:1:1) and magnitude of the splitting (70 MHz, 2.4 mT) is consistent with coupling to a (I = 1) ^{14}N-nucleus (I = 1). These spectroscopic properties are consistent with an N-atom centered organic radical. As a similar signal was observed in reactions of

Significantly, this signal is only observed when samples are examined immediately (within ~1 hour of preparation). Re-examination of samples stored in liquid nitrogen overnight show a complete loss of this feature. This suggests that the observed species is either highly reactive, remains volatile at 77 K, or both. Based on these properties, and similar signals observed upon stoichiometric treatment of the peroxo adduct with nitrosonium[38], we conclude this feature is diagnostic of free NO_2-radical formed during turnover.

A low intensity signal consistent with mononuclear Cu(II) can be observed near g ~ 2 in samples treated with NO^+. As the amount varies sample-to-sample, and quantitation of the Cu-signal by quantitative simulation (~ 50 μM) does not exceed 3% relative to the total iron in the sample, this species was considered an impurity present in solutions of the nitrosonium and not considered further.

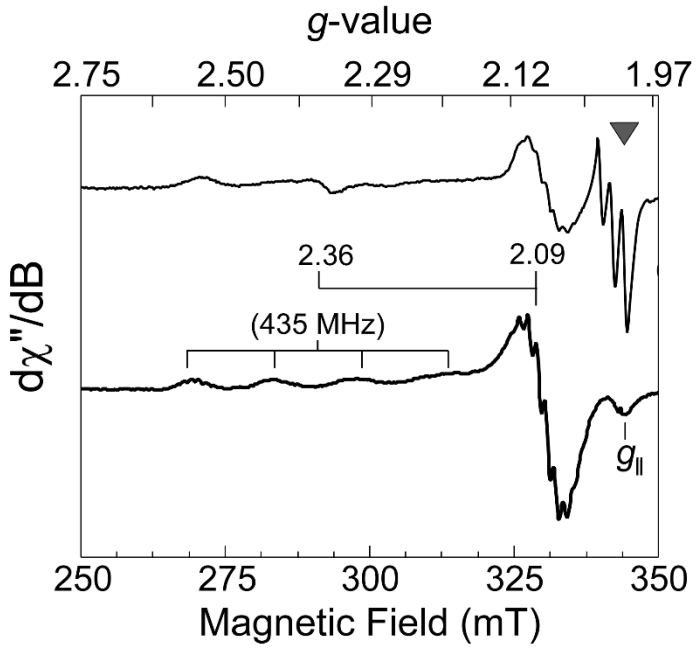

Fig. S9 An expansion of the g ~ 2 region illustrating the N-centered radical (▼) and Cu(II)-impurity present in samples treated with NO^+. The features labeled "g_I" at g ~ 2.0 represents lowest numerical g-value observed for the high-spin axial heme. The Cu(II)-impurity exhibits g_z- [2.09, 2.08, 2.37] and A_z-values [- , - , 435] typical of 4-coordinate N/O-atom complexes.[12] While not shown, simulations of the Cu(II) impurity exhibit multiline splitting consistent with multiple coupled ^{14}N-coupling (45 MHz) nuclei. *Instrumental parameters*: microwave frequency, 9.63 GHz, microwave power, 20 μW, temperature, 20 K; modulation amplitude, 0.9 mT.

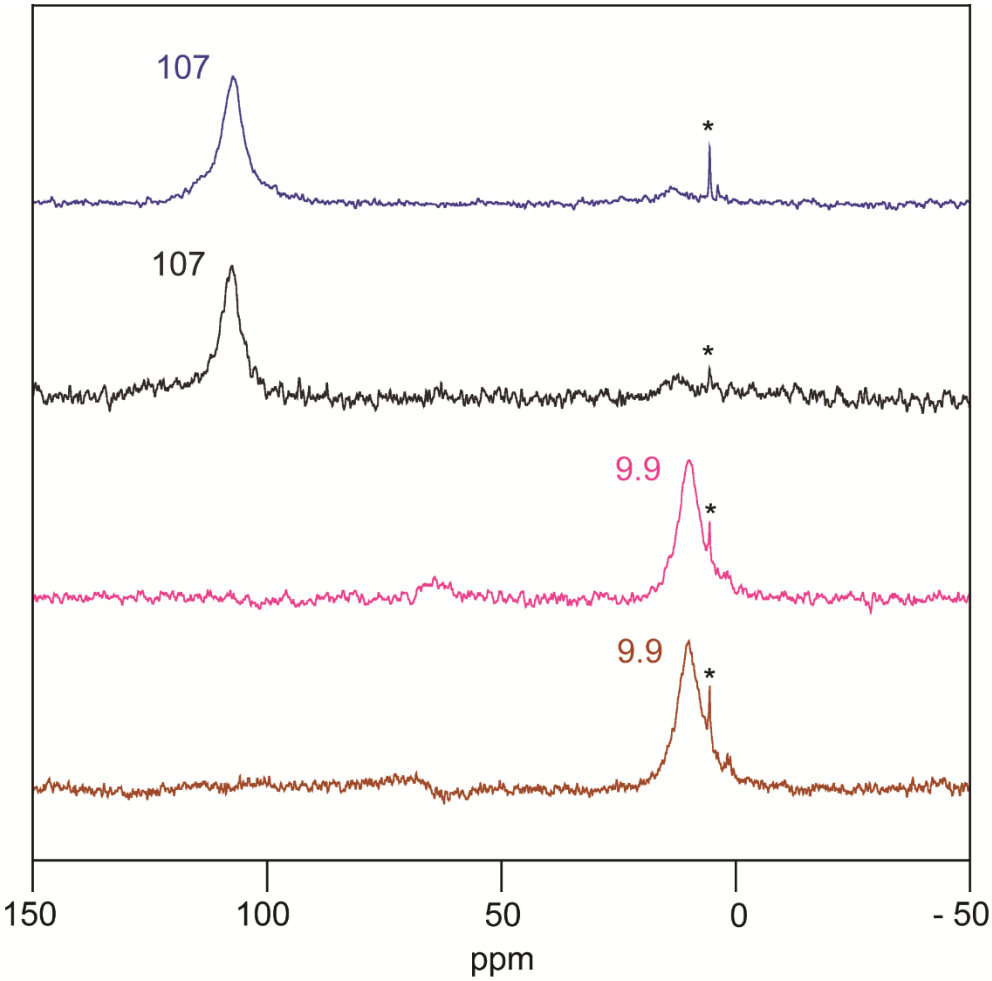

Fig. S10 ^{2}H NMR spectral data in 9:1 DCM:THF for $[(F_{20}TPP\text{-}d_8)Fe^{III}(O_2^{2-})]^{-}$ after addition of 4 equiv $NOPF_6$ (brown), standard $[(F_{20}TPP\text{-}d_8)Fe^{III}(NO_2)_2]^{+}$(pink), the final heme product at room temperature (black) and authentic ($[(F_{20}TPP\text{-}d_8)Fe^{III}SbF_6]$) (blue).

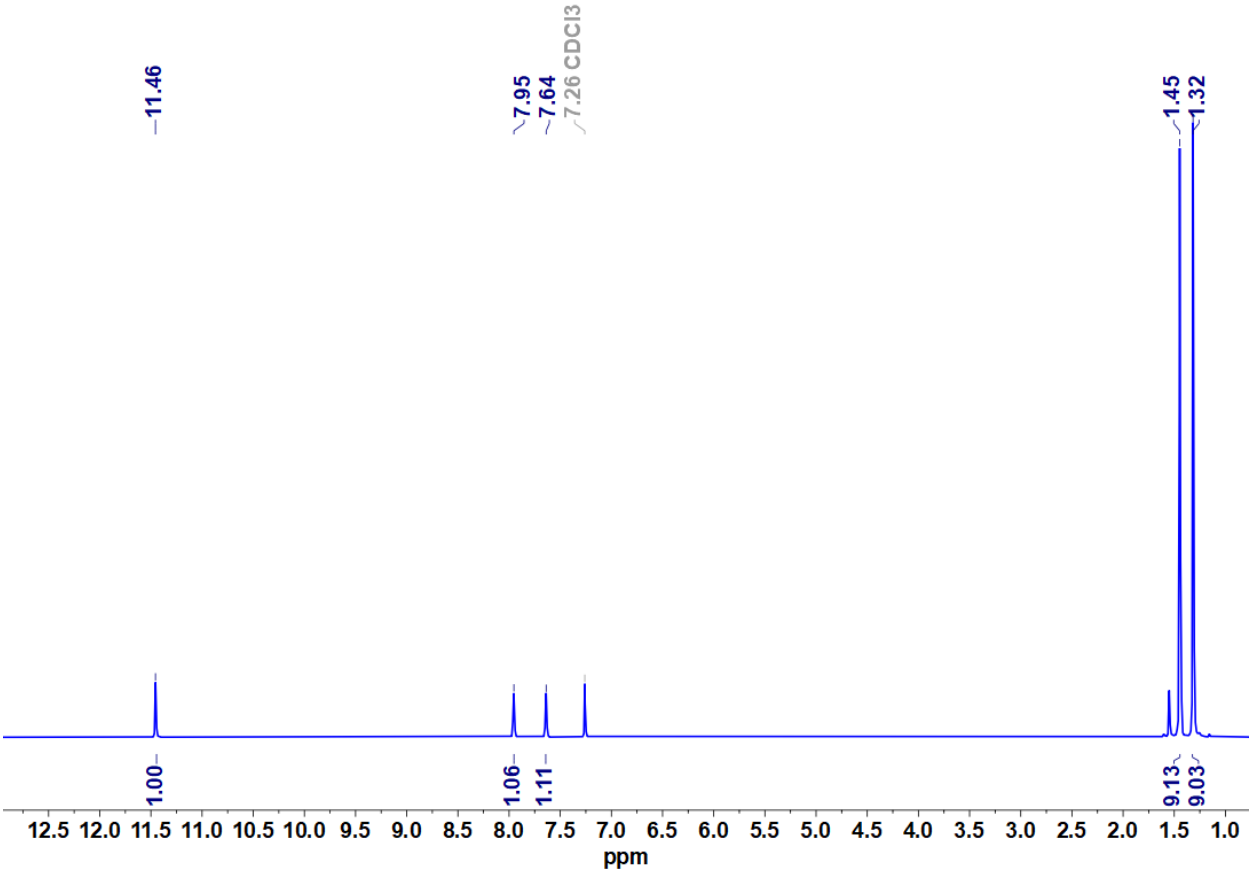

Fig. S11 ^{1}H NMR spectra of purified final 2,4-bis(*tert*-butyl)-6-nitrophenol product in $CDCl_3$ after bulk reaction of $[(F_{20}TPP)Fe^{III}(O_2^{2-})]^-$ with addition of 4 equiv $NOPF_6$ and addition of 20 equiv 2,4-DTBP.

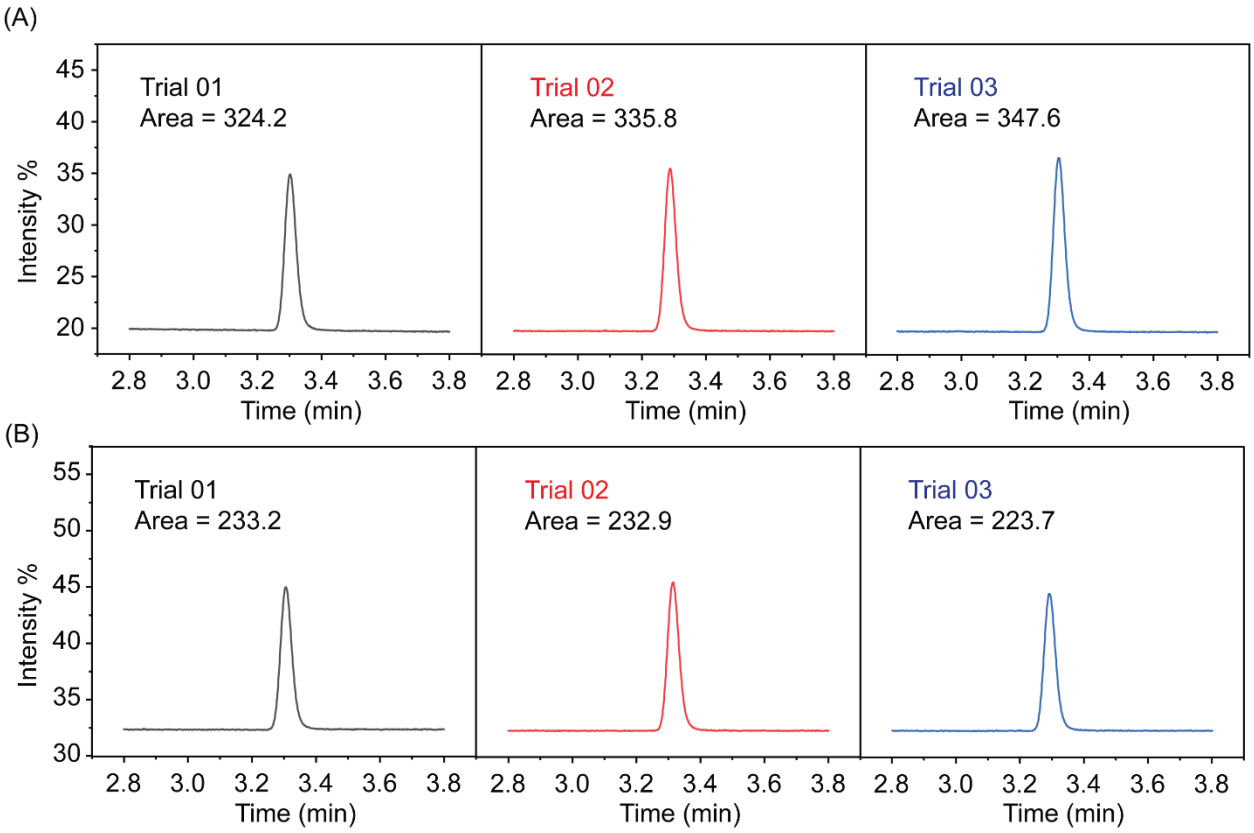

Fig. S12 GC-ECD (A) chromatograms for three standard N_2O (B) chromatograms for triplicated experimental N_2O product.

Control Experiment:

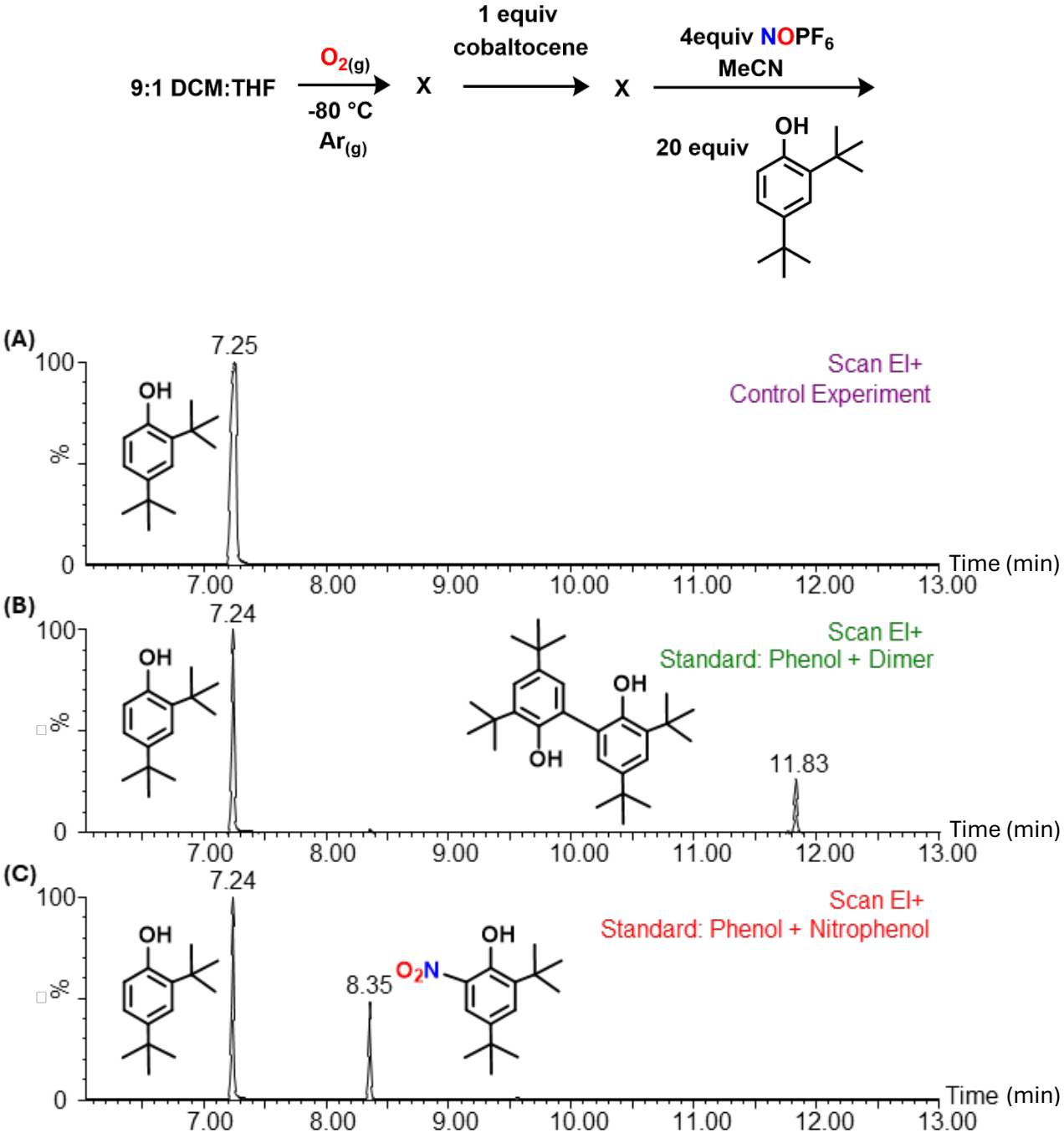

Fig. S13 GC-MS chromatograms for (A) Control Experiment (B) Standard for 2,4-DTBP + 3,3',5,5'-tetra-*tert*-butyl[1,1'-biphenyl]-2,2'-diol (11.83 min) (C) Standard for 2,4-DTBP (7.24 min) + 2,4-di-*tert*-butyl-6-nitrophenol (8.35 min).

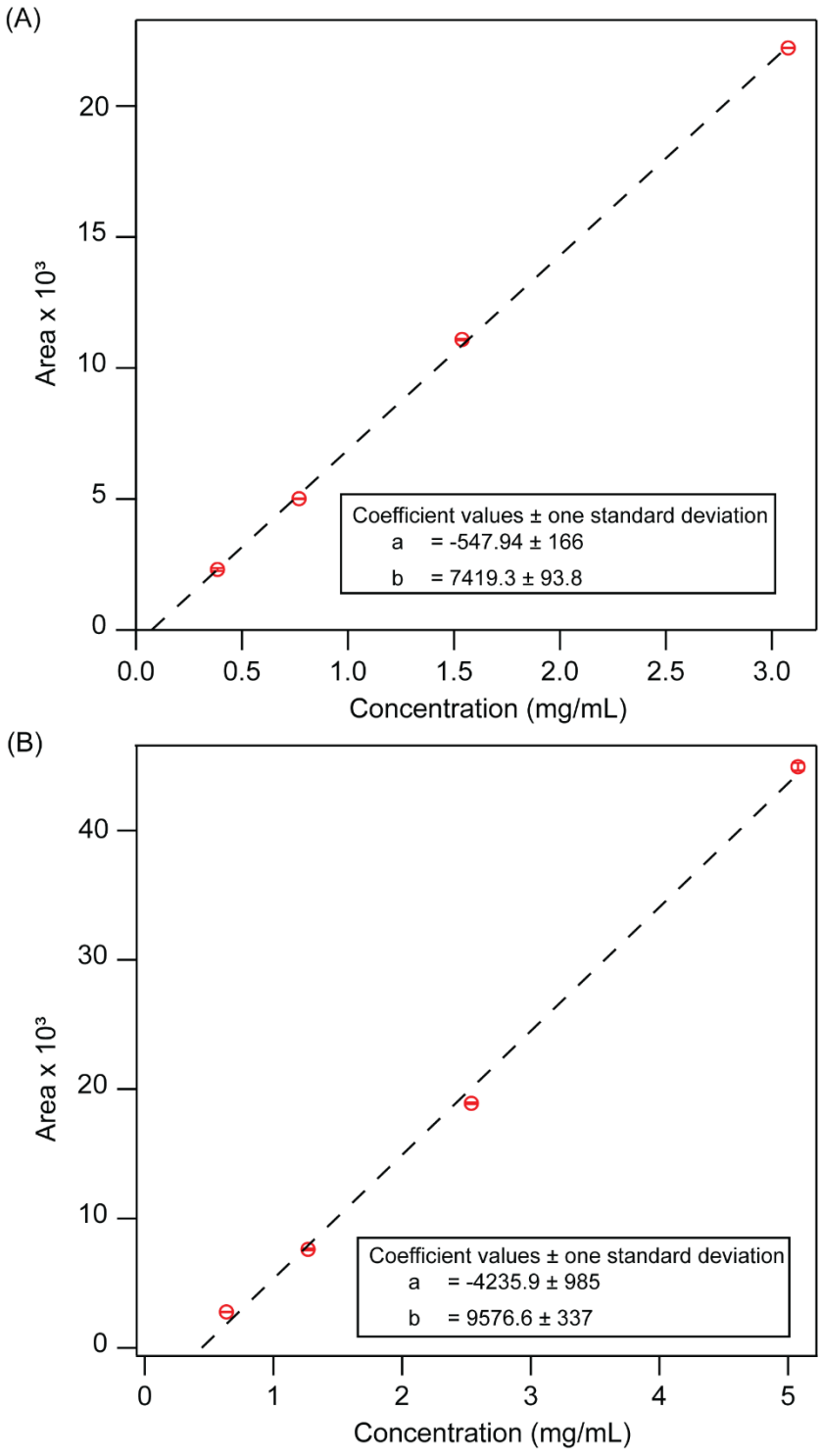

Fig. S14 Calibration curve for (A) 2,4-di-*tert*-butyl-6-nitrophenol and (B) 3,3',5,5'-tetra-*tert*-butylbiphenyl-2,2'-diol.

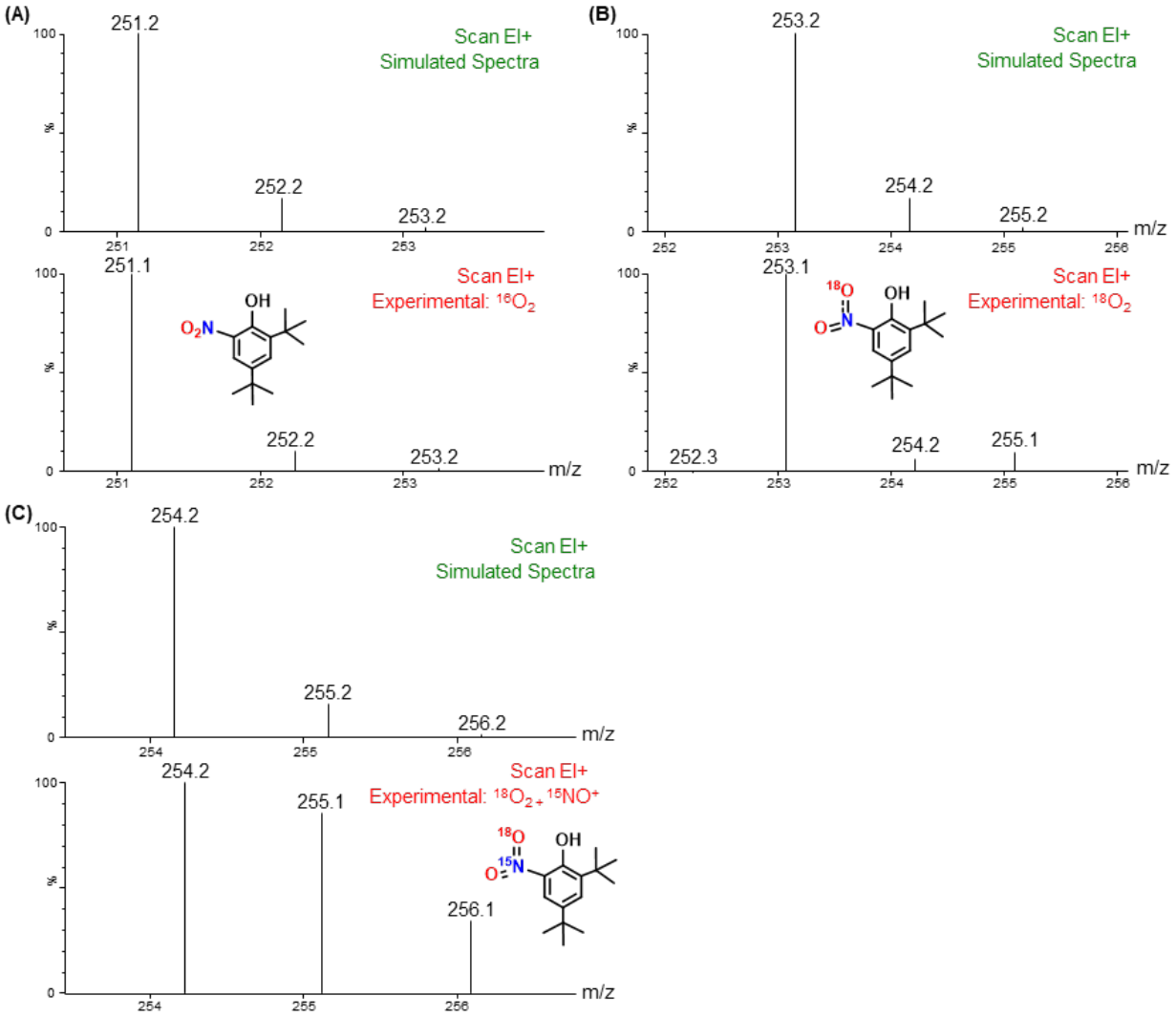

Fig. S15 (A) Simulated spectrum of $C_{14}H_{21}NO_3$ showing $[M]^+$ m/z = 251.2 (top) and GC-MS spectrum of $C_{14}H_{21}NO_3$ product showing $[M]^+$ m/z = 251.2 (bottom) (B) Simulated spectrum of $C_{14}H_{21}N^{18}OO_2$ showing $[M]^+$ m/z = 253.2 (top) and GC-MS spectrum of $C_{14}H_{21}N^{18}OO_2$ product showing $[M]^+$ m/z = 253.2 (bottom). (C) Simulated spectrum of $C_{14}H_{21}{}^{15}N^{18}OO_2$ showing $[M]^+$ m/z = 254.2 (top) and GC-MS spectrum of $C_{14}H_{21}{}^{15}N^{18}OO_2$ product showing $[M]^+$ m/z = 254.2 (bottom).

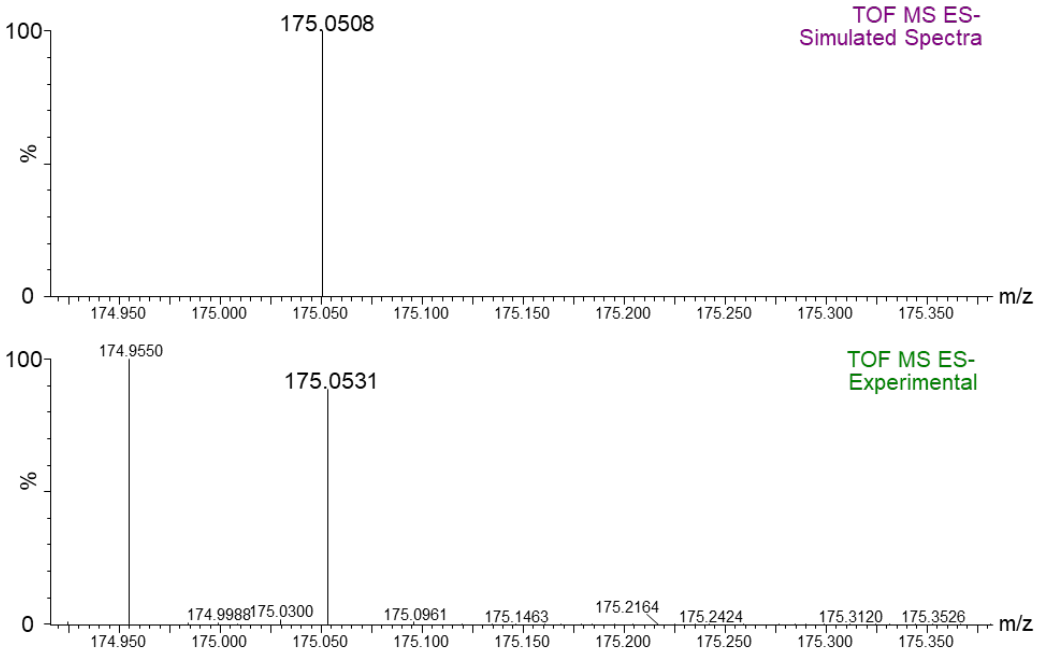

Fig. S16 Simulated spectrum of $C_9H_8N_2O_2$ showing $[M-H]^-$ m/z = 175.0508 (top) and ESI-MS spectrum of $C_9H_8N_2O_2$ product showing $[M-H]^-$ m/z = 175.0531 (bottom).

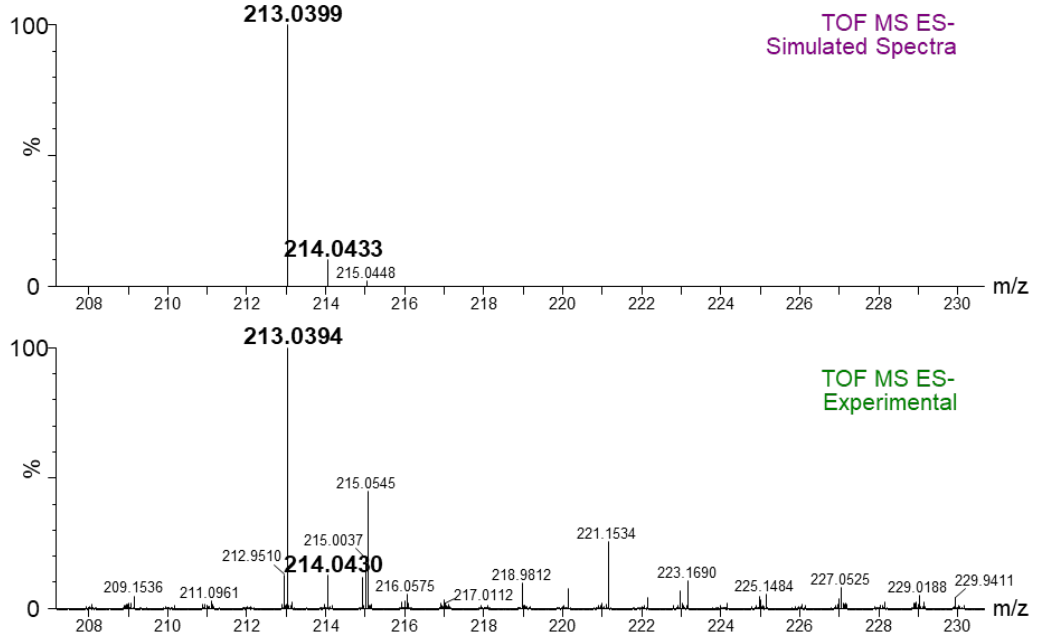

Fig. S17 Simulated spectrum of $C_9H_{10}O_6$ showing $[M-H]^-$ m/z = 213.0399 (top) and ESI-MS spectrum of $C_9H_{10}O_6$ product showing $[M-H]^-$ m/z = 213.0394 (bottom).

Table S2. N_2O, nitrite and nitrate yields for different experimental reactions and controls

Reaction	N_2O	NO_2^-	NO_3^-
DCM:THF (9:1) solvents + O_2 + 1 equiv cobaltocene + 4 equiv $NOPF_6$	84%	0%	0%
$[(F_{20}TPP)Fe^{III}(O_2^{2-})]^-$ + 4 equiv $NOPF_6$	77%	0%	0%
$[(F_{20}TPP)Fe^{III}(O_2^{2-})]^-$ + 4 equiv $NOPF_6$ + 10 equiv 2,4-DTBP	68%	0%	0%
THF + 4 equiv $NOPF_6$	83%	0%	0%
*All experiments were performed under identical conditions.			

Cartesian coordinates

NO^+

N 0.000000 0.000000 -0.567038

O 0.000000 0.000000 0.496158

$^{\bullet}NO_2$

O 1.0991070000 -0.1402270000 -0.0000000000

N 0.0000000000 0.3198040000 0.0000000000

O -1.0991070000 -0.1396020000 0.0000000000

A

C	-1.0119520000	2.9054420000	0.0225950000
N	0.0628940000	2.0622830000	0.0045240000
C	1.1875420000	2.8371850000	0.0624440000
C	0.8125090000	4.2419020000	0.0935110000
C	-0.5518420000	4.2839440000	0.0763800000
Fe	0.0006740000	-0.0008180000	-0.5697190000
N	2.0649910000	-0.0653510000	0.0873230000
C	2.8344400000	-1.1888400000	0.1590890000
C	4.2361240000	-0.8176530000	0.3005150000
C	4.2798560000	0.5459160000	0.3021440000
C	2.9050550000	1.0063600000	0.1602100000
C	2.3574280000	-2.5154280000	0.1254760000
C	3.3819650000	-3.5995500000	0.1884940000
C	3.5288580000	-4.4074490000	1.3211870000
C	4.4922730000	-5.4131010000	1.3923940000
C	5.3433720000	-5.6276040000	0.3085650000
C	5.2240190000	-4.8368710000	-0.8340060000
C	4.2505600000	-3.8394440000	-0.8819340000
F	2.7353640000	-4.2255260000	2.3793870000
F	4.6088050000	-6.1646100000	2.4874720000
F	6.2676720000	-6.5831080000	0.3648210000
F	6.0358090000	-5.0427400000	-1.8710730000
F	4.1644720000	-3.1005560000	-1.9893040000
C	2.5134030000	2.3606500000	0.1279790000
C	3.6023430000	3.3798190000	0.1902370000
C	3.7977610000	4.1777670000	1.3226990000
C	4.8136560000	5.1305150000	1.3899320000
C	5.6691600000	5.3012020000	0.3018300000

C	5.5032740000	4.5178170000	-0.8399840000
C	4.4784450000	3.5730660000	-0.8835940000
F	3.0001630000	4.0384870000	2.3843370000
F	4.9748440000	5.8739920000	2.4848250000
F	6.6415490000	6.2079840000	0.3532060000
F	6.3193840000	4.6815240000	-1.8812270000
F	4.3475570000	2.8413970000	-1.9914260000
C	-2.3676960000	2.5143210000	0.0322580000
C	-2.8461030000	1.1880270000	0.0554300000
N	-2.0727430000	0.0645720000	0.0874810000
C	-2.9163860000	-1.0073410000	0.0561800000
C	-4.2981820000	-0.5465770000	0.0162860000
C	-4.2545590000	0.8164010000	0.0158180000
C	-2.5234320000	-2.3614730000	0.0325910000
C	-1.1951210000	-2.8376240000	0.0224850000
N	-0.0697270000	-2.0636890000	0.0032970000
C	1.0043140000	-2.9076060000	0.0599170000
C	0.5419230000	-4.2860180000	0.0921520000
C	-0.8224110000	-4.2423280000	0.0758760000
C	-3.3877480000	3.6033050000	0.0165080000
C	-3.5620790000	4.4248040000	-1.1032550000
C	-4.5149930000	5.4425190000	-1.1323440000
C	-5.3267260000	5.6572210000	-0.0187580000
C	-5.1772450000	4.8558060000	1.1127390000
C	-4.2151060000	3.8465980000	1.1186330000
F	-2.8064590000	4.2446350000	-2.1881380000
F	-4.0968580000	3.1021740000	2.2204780000
F	-5.9490690000	5.0631910000	2.1798320000
F	-6.2411610000	6.6236950000	-0.0357570000
F	-4.6594950000	6.2055080000	-2.2158810000

O	-0.6848080000	0.0153040000	-2.5048130000
C	-3.6090400000	-3.3850040000	0.0136790000
C	-4.4503490000	-3.5816600000	1.1146120000
C	-5.4682080000	-4.5346670000	1.1067280000
C	-5.6610270000	-5.3260560000	-0.0252930000
C	-4.8382220000	-5.1556390000	-1.1383730000
C	-3.8292150000	-4.1936490000	-1.1073160000
F	-4.2907660000	-2.8464030000	2.2173600000
F	-6.2512360000	-4.6994360000	2.1731160000
F	-6.6271380000	-6.2408300000	-0.0432200000
F	-5.0244450000	-5.9082810000	-2.2227500000
F	-3.0637990000	-4.0555140000	-2.1915420000
H	1.4970140000	5.0864180000	0.1308730000
H	-1.1842410000	5.1682150000	0.1129410000
H	1.1721060000	-5.1717810000	0.1291850000
H	-1.5089380000	-5.0852910000	0.1132050000
H	5.0729640000	-1.5052690000	0.4021900000
H	5.1587470000	1.1785560000	0.4056300000
H	-5.1829660000	-1.1779510000	-0.0254500000
H	-5.0973910000	1.5028140000	-0.0264920000
O	0.6606490000	-0.0269810000	-2.5170270000

B

Fe	0.0699620000	0.0018760000	0.0356640000
N	0.0757640000	2.0086260000	-0.1964400000
N	2.0767510000	0.0047230000	-0.1966420000
N	0.0696260000	-2.0034850000	-0.2091190000
N	-1.9341120000	0.0026790000	-0.2251180000
C	-1.0246400000	2.8388080000	-0.1819510000

C	-0.6079070000	4.2192010000	-0.1856250000
C	0.7542690000	4.2208260000	-0.1849290000
C	1.1740170000	2.8411000000	-0.1969960000
C	2.9090610000	1.1024880000	-0.2351330000
C	4.2863920000	0.6817290000	-0.3061250000
C	4.2844840000	-0.6805720000	-0.2938080000
C	2.9059760000	-1.0962200000	-0.2181950000
C	1.1686730000	-2.8349170000	-0.1920420000
C	0.7498650000	-4.2149370000	-0.1912400000
C	-0.6120770000	-4.2144170000	-0.2176630000
C	-1.0300230000	-2.8342080000	-0.2136710000
C	-2.7667370000	-1.0960720000	-0.2027790000
C	-4.1446610000	-0.6759790000	-0.1500070000
C	-4.1427450000	0.6865770000	-0.1431670000
C	-2.7642890000	1.1033320000	-0.1904540000
C	-2.3606680000	2.4383870000	-0.1736680000
C	2.5104650000	2.4397710000	-0.2201900000
C	2.5051160000	-2.4328390000	-0.1970640000
C	-2.3659700000	-2.4326280000	-0.2039640000
H	1.4137210000	-5.0750680000	-0.1725690000
H	-1.2771770000	-5.0736740000	-0.2394050000
H	1.4180740000	5.0812320000	-0.1761910000
H	-1.2742850000	5.0777270000	-0.1927110000
H	5.1443760000	1.3454470000	-0.3719190000
H	5.1405510000	-1.3477670000	-0.3481590000
H	-5.0005760000	1.3515650000	-0.0921830000
H	-5.0041390000	-1.3395140000	-0.1072150000
O	0.0863980000	0.0121800000	1.9877960000
C	-3.4140010000	3.4913760000	-0.1192350000
C	-4.2502530000	3.7448510000	-1.2111770000

C	-5.2466380000	4.7186430000	-1.1633280000
C	-5.4180570000	5.4696630000	-0.0002130000
C	-4.5969590000	5.2403680000	1.1041680000
C	-3.6102810000	4.2575820000	1.0349210000
F	-4.1096310000	3.0400430000	-2.3352900000
F	-6.0299330000	4.9377850000	-2.2173780000
F	-6.3626610000	6.4020260000	0.0553050000
F	-4.7618630000	5.9565810000	2.2140830000
F	-2.8409430000	4.0593120000	2.1047110000
C	3.5677120000	3.4906470000	-0.2328750000
C	3.7765280000	4.3008270000	-1.3538940000
C	4.7635060000	5.2851310000	-1.3763930000
C	5.5729450000	5.4723140000	-0.2555550000
C	5.3896160000	4.6772790000	0.8761630000
C	4.3937980000	3.7014220000	0.8764740000
F	3.0172050000	4.1437950000	-2.4397310000
F	4.9393390000	6.0423700000	-2.4571770000
F	6.5175440000	6.4060790000	-0.2661800000
F	6.1617620000	4.8561580000	1.9455360000
F	4.2423640000	2.9547510000	1.9705030000
C	3.5627570000	-3.4834660000	-0.1892210000
C	3.7863580000	-4.3022110000	-1.3011230000
C	4.7740270000	-5.2860500000	-1.3032770000
C	5.5697660000	-5.4635210000	-0.1711130000
C	5.3722060000	-4.6592310000	0.9516300000
C	4.3757900000	-3.6841570000	0.9316100000
F	3.0410630000	-4.1542350000	-2.3979250000
F	4.9636290000	-6.0519390000	-2.3756100000
F	6.5146690000	-6.3970050000	-0.1624910000
F	6.1314470000	-4.8285300000	2.0317400000

F	4.2108280000	-2.9283120000	2.0173130000
C	-3.4211610000	-3.4846220000	-0.1697310000
C	-4.2515580000	-3.7210720000	-1.2699770000
C	-5.2479970000	-4.6956590000	-1.2427310000
C	-5.4262060000	-5.4642080000	-0.0921130000
C	-4.6115130000	-5.2517350000	1.0204200000
C	-3.6246840000	-4.2680520000	0.9713690000
F	-4.1046070000	-2.9991590000	-2.3822550000
F	-6.0251820000	-4.8986120000	-2.3044380000
F	-6.3711010000	-6.3971100000	-0.0559670000
F	-4.7828140000	-5.9843340000	2.1185160000
F	-2.8613250000	-4.0850520000	2.0489040000
O	-0.8527100000	-0.8776570000	2.5208290000
N	-2.0297530000	-0.2748430000	2.9590540000
O	-2.0938660000	0.8932950000	2.8094580000

C

C	-1.1001630000	2.8342650000	0.0407470000
N	-0.0029160000	2.0020720000	0.0694780000
C	1.0937600000	2.8356510000	0.0774310000
C	0.6763130000	4.2179570000	0.0693750000
C	-0.6844690000	4.2170320000	0.0580390000
Fe	0.0014420000	-0.0000110000	-0.1958430000
N	1.9963560000	0.0000200000	0.0968170000
C	2.8286970000	-1.0970380000	0.1276950000
C	4.2085940000	-0.6802830000	0.2113170000
C	4.2085300000	0.6805130000	0.2114300000
C	2.8285820000	1.0971670000	0.1278830000

C	2.4288690000	-2.4331080000	0.1082180000
C	3.4864420000	-3.4841380000	0.1304050000
C	3.6908040000	-4.2868630000	1.2574460000
C	4.6791680000	-5.2694870000	1.2915100000
C	5.4947470000	-5.4625040000	0.1762040000
C	5.3159550000	-4.6748720000	-0.9613360000
C	4.3185340000	-3.7006560000	-0.9730130000
F	2.9259060000	-4.1241560000	2.3385900000
F	4.8504740000	-6.0196500000	2.3780920000
F	6.4409970000	-6.3946870000	0.1975940000
F	6.0942160000	-4.8591050000	-2.0255840000
F	4.1722890000	-2.9606600000	-2.0725050000
C	2.4286590000	2.4332130000	0.1085130000
C	3.4861530000	3.4843350000	0.1308080000
C	3.6904780000	4.2869730000	1.2579170000
C	4.6788130000	5.2696180000	1.2920580000
C	5.4943880000	5.4627590000	0.1767630000
C	5.3155970000	4.6752580000	-0.9608620000
C	4.3181760000	3.7010340000	-0.9726280000
F	2.9255630000	4.1241460000	2.3390210000
F	4.8501100000	6.0197080000	2.3786970000
F	6.4406200000	6.3949580000	0.1982660000
F	6.0938430000	4.8596010000	-2.0250960000
F	4.1719150000	2.9611840000	-2.0722150000
C	-2.4351330000	2.4325120000	-0.0001870000
C	-2.8370590000	1.0969520000	-0.0102150000
N	-2.0057030000	-0.0000790000	0.0407530000
C	-2.8369620000	-1.0971850000	-0.0101320000
C	-4.2175590000	-0.6805910000	-0.0835680000
C	-4.2176120000	0.6802450000	-0.0836360000

C	-2.4349510000	-2.4327150000	-0.0000600000
C	-1.0999420000	-2.8343840000	0.0407580000
N	-0.0027440000	-2.0021160000	0.0693790000
C	1.0939900000	-2.8356230000	0.0772000000
C	0.6766350000	-4.2179520000	0.0691120000
C	-0.6841500000	-4.2171210000	0.0579800000
C	-3.4892740000	3.4863710000	-0.0452320000
C	-3.6777730000	4.2783540000	-1.1827630000
C	-4.6624260000	5.2640110000	-1.2374580000
C	-5.4891870000	5.4717590000	-0.1330940000
C	-5.3252220000	4.6959610000	1.0147340000
C	-4.3313970000	3.7187930000	1.0470930000
F	-2.9018190000	4.1023990000	-2.2529570000
F	-4.1985340000	2.9904530000	2.1569490000
F	-6.1136330000	4.8944950000	2.0690860000
F	-6.4319690000	6.4067970000	-0.1743620000
F	-4.8195480000	6.0034970000	-2.3332900000
O	0.0149160000	0.0000410000	-1.7924160000
C	-3.4890660000	-3.4866190000	-0.0449530000
C	-4.3309180000	-3.7191450000	1.0475580000
C	-5.3247870000	-4.6962760000	1.0153250000
C	-5.4890380000	-5.4719490000	-0.1325470000
C	-4.6625690000	-5.2640760000	-1.2371060000
C	-3.6778540000	-4.2784750000	-1.1825260000
F	-4.1977590000	-2.9909270000	2.1574590000
F	-6.1129430000	-4.8949240000	2.0698430000
F	-6.4318570000	-6.4069580000	-0.1736860000
F	-4.8199850000	-6.0034390000	-2.3329820000
F	-2.9021530000	-4.1024180000	-2.2528810000
H	1.3414730000	5.0774050000	0.0726840000

H	-1.3512990000	5.0752170000	0.0645110000
H	1.3418430000	-5.0773670000	0.0722920000
H	-1.3508970000	-5.0753620000	0.0645210000
H	5.0643650000	-1.3466310000	0.2790630000
H	5.0642300000	1.3469370000	0.2792960000
H	-5.0746050000	-1.3462720000	-0.1407820000
H	-5.0747080000	1.3458600000	-0.1408940000

D

O	-0.0883050000	0.0680140000	2.0704850000
Fe	-0.0407910000	0.0313360000	-0.1911540000
N	-1.9771790000	-0.3883040000	-0.1458890000
C	-2.5588360000	-1.6290700000	0.0456090000
C	-3.9909370000	-1.5117890000	0.0172060000
C	-4.2798400000	-0.1974220000	-0.2136380000
C	-3.0255690000	0.5005660000	-0.2944910000
C	-1.8836730000	-2.8412820000	0.1827260000
C	-0.5015740000	-2.9572260000	0.0413760000
N	0.3858490000	-1.9105520000	-0.1477920000
C	1.6250650000	-2.4996750000	-0.3498990000
C	1.5027110000	-3.9297090000	-0.2983340000
C	0.1967680000	-4.2111650000	-0.0162300000
C	-2.9178330000	1.8857100000	-0.4170020000
C	-1.7038150000	2.5603810000	-0.2930740000
N	-0.4596140000	1.9729820000	-0.1436810000
C	0.4284710000	3.0153080000	0.0577800000
C	-0.2752530000	4.2689240000	0.0502350000
C	-1.5858150000	3.9904060000	-0.2087930000
C	1.8132450000	2.8980820000	0.1751290000

C	2.4854100000	1.6859040000	0.0175010000
N	1.8991360000	0.4434920000	-0.1566140000
C	2.9463920000	-0.4426540000	-0.3549370000
C	4.1990950000	0.2580150000	-0.3089070000
C	3.9151000000	1.5705010000	-0.0590210000
C	2.8351300000	-1.8244200000	-0.4964640000
C	4.0833190000	-2.6100400000	-0.7079440000
C	4.7407640000	-2.5965860000	-1.9415600000
C	5.9209020000	-3.3091940000	-2.1496950000
C	6.4682390000	-4.0513460000	-1.1022010000
C	5.8348230000	-4.0780750000	0.1412350000
C	4.6558820000	-3.3576570000	0.3261650000
F	4.2398820000	-1.8855910000	-2.9523460000
F	6.5247610000	-3.2861470000	-3.3345860000
F	7.5909970000	-4.7337110000	-1.2886400000
F	6.3599700000	-4.7833550000	1.1392640000
F	4.0699730000	-3.3918930000	1.5237160000
C	-2.6859790000	-4.0748880000	0.4209990000
C	-3.2414540000	-4.3354690000	1.6774900000
C	-3.9937910000	-5.4835470000	1.9216220000
C	-4.2054460000	-6.3979790000	0.8888700000
C	-3.6640940000	-6.1612320000	-0.3755360000
C	-2.9156080000	-5.0060980000	-0.5964230000
F	-3.0558170000	-3.4723570000	2.6768480000
F	-2.4061710000	-4.8013300000	-1.8117360000
F	-3.8678480000	-7.0326080000	-1.3596730000
F	-4.9213290000	-7.4932870000	1.1093970000
F	-4.5088330000	-5.7104840000	3.1266400000
C	-4.1727170000	2.6679420000	-0.6043480000
C	-4.8493850000	2.6468420000	-1.8280970000

C	-6.0433360000	3.3412620000	-2.0170090000
C	-6.5847400000	4.0757950000	-0.9610890000
C	-5.9319650000	4.1113740000	0.2718580000
C	-4.7390820000	3.4092310000	0.4375190000
F	-4.3555180000	1.9421080000	-2.8467670000
F	-6.6655140000	3.3091330000	-3.1921590000
F	-7.7203070000	4.7412860000	-1.1297120000
F	-6.4508830000	4.8088360000	1.2785680000
F	-4.1372600000	3.4527770000	1.6268160000
C	2.6256500000	4.1241030000	0.4136860000
C	2.7837660000	5.1051490000	-0.5707100000
C	3.5486900000	6.2490970000	-0.3486960000
C	4.1834810000	6.4236310000	0.8817690000
C	4.0507820000	5.4562290000	1.8787870000
C	3.2790570000	4.3214030000	1.6349300000
F	2.1922180000	4.9592170000	-1.7571130000
F	3.6798910000	7.1688430000	-1.3004170000
F	4.9137490000	7.5090060000	1.1030630000
F	4.6570910000	5.6219430000	3.0508130000
F	3.1726540000	3.4064110000	2.5993180000
H	2.3158130000	-4.6356860000	-0.4436570000
H	-0.2564300000	-5.1894820000	0.1205490000
H	0.1739360000	5.2455800000	0.2088430000
H	-2.4046950000	4.6969500000	-0.3134560000
H	4.6147300000	2.3960880000	0.0430320000
H	5.1765440000	-0.2008600000	-0.4335090000
H	-5.2595630000	0.2653020000	-0.2995620000
H	-4.6881710000	-2.3362970000	0.1413010000
N	0.7542480000	-0.4558250000	2.7579670000
O	1.7300500000	-1.0685210000	2.5090800000

E

C	-3.7601970000	-4.2472980000	-1.2266570000
C	-3.5496960000	-3.4343700000	-0.1081840000
C	-4.3858810000	-3.6259550000	0.9968970000
C	-5.3949780000	-4.5875590000	0.9954930000
C	-5.5807800000	-5.3865090000	-0.1334250000
C	-4.7616150000	-5.2168110000	-1.2504840000
C	-2.4763820000	-2.4000870000	-0.0897990000
C	-1.1480030000	-2.8168350000	-0.0298080000
N	-0.0321100000	-1.9970210000	0.0003560000
C	1.0575050000	-2.8516490000	0.0318770000
C	0.6150440000	-4.2185930000	0.0131880000
C	-0.7486890000	-4.1970270000	-0.0090550000
Fe	0.0003080000	-0.0000570000	-0.0011870000
N	-1.9951950000	0.0314130000	-0.0873500000
C	-2.8129170000	1.1478410000	-0.1302680000
C	-4.1900630000	0.7491690000	-0.2238150000
C	-4.2122240000	-0.6148260000	-0.2238190000
C	-2.8486820000	-1.0580350000	-0.1304710000
C	-2.3979040000	2.4772750000	-0.0902320000
C	-3.4381440000	3.5449340000	-0.1039550000
C	-3.6303290000	4.3634540000	-1.2215780000
C	-4.6006520000	5.3643100000	-1.2392150000
C	-5.4085980000	5.5581220000	-0.1179140000
C	-5.2400320000	4.7546020000	1.0106250000
C	-4.2622230000	3.7612300000	1.0055720000
C	2.3982380000	-2.4769410000	0.0922930000
C	3.4385000000	-3.5443030000	0.1103850000

C	3.6276820000	-4.3603390000	1.2302770000
C	4.5978300000	-5.3613650000	1.2525420000
C	5.4081290000	-5.5579460000	0.1333980000
C	5.2415590000	-4.7577090000	-0.9977650000
C	4.2639350000	-3.7640970000	-0.9972760000
F	2.8628640000	-4.1940560000	2.3102510000
F	4.7565130000	-6.1246450000	2.3302950000
F	6.3366090000	-6.5058410000	0.1444290000
F	6.0139150000	-4.9450570000	-2.0642760000
F	4.1275030000	-3.0081470000	-2.0875080000
F	-2.8682750000	4.1999160000	-2.3039310000
F	-4.7612850000	6.1306500000	-2.3145010000
F	-6.3363660000	6.5067380000	-0.1244380000
F	-6.0105640000	4.9386140000	2.0790390000
F	-4.1233430000	3.0032000000	2.0940620000
F	-4.2294710000	-2.8734100000	2.0867860000
F	-6.1760850000	-4.7488940000	2.0599210000
F	-6.5366910000	-6.3066660000	-0.1450830000
F	-4.9389700000	-5.9784030000	-2.3264410000
F	-2.9879810000	-4.1073350000	-2.3051660000
N	0.0323480000	1.9969800000	-0.0022760000
C	-1.0571080000	2.8517330000	-0.0317690000
C	-0.6143590000	4.2185920000	-0.0136880000
C	0.7493920000	4.1969700000	0.0049470000
C	1.1483070000	2.8167510000	0.0255990000
C	2.4766040000	2.4000200000	0.0840770000
C	3.5497460000	3.4343920000	0.1006030000
C	3.7631810000	4.2457260000	1.2194760000
C	4.7649130000	5.2149570000	1.2418130000
C	5.5809020000	5.3861110000	0.1226390000

C	5.3919090000	4.5887220000	-1.0068950000
C	4.3827980000	3.6270840000	-1.0065950000
F	2.9930830000	4.1048020000	2.2993760000
F	4.9451470000	5.9752890000	2.3181930000
F	6.5364680000	6.3066700000	0.1326260000
F	6.1698860000	4.7515590000	-2.0733970000
F	4.2239140000	2.8749060000	-2.0963730000
N	1.9955800000	-0.0315060000	0.0854830000
C	2.8133280000	-1.1477110000	0.1305200000
C	4.1905510000	-0.7488690000	0.2234370000
C	4.2125730000	0.6151930000	0.2208580000
C	2.8489990000	1.0579930000	0.1263980000
H	1.4269280000	5.0466840000	0.0058440000
H	-1.2643830000	5.0893030000	-0.0169560000
H	1.2652550000	-5.0892240000	0.0175580000
H	-1.4259220000	-5.0468500000	-0.0123940000
H	5.0363360000	-1.4275320000	0.2921240000
H	5.0796900000	1.2664720000	0.2871820000
H	-5.0795420000	-1.2657340000	-0.2913000000
H	-5.0355870000	1.4282160000	-0.2909460000

TS1

C	2.0853560000	-5.0166400000	1.4266070000
C	2.1364040000	-4.3611090000	0.1919900000
C	2.8289290000	-4.9923400000	-0.8455680000
C	3.4521180000	-6.2269220000	-0.6690120000
C	3.3858410000	-6.8578080000	0.5734890000
C	2.6991490000	-6.2525280000	1.6262740000
C	1.4688000000	-3.0424270000	-0.0009130000

C	0.0758730000	-3.0151980000	-0.0557240000
N	-0.7040770000	-1.8892910000	-0.1945690000
C	-2.0032510000	-2.3424220000	-0.2607260000
C	-2.0381370000	-3.7833070000	-0.1756110000
C	-0.7488610000	-4.2003640000	-0.0409600000
Fe	-0.0722290000	0.0101190000	-0.0243020000
O	-0.0814110000	0.0078900000	1.6491410000
C	-3.1440440000	-1.5465660000	-0.3691290000
C	-4.4662670000	-2.2253810000	-0.4817590000
C	-4.8151690000	-2.9317160000	-1.6376630000
C	-6.0447310000	-3.5763270000	-1.7631220000
C	-6.9601430000	-3.5197120000	-0.7119780000
C	-6.6392010000	-2.8242070000	0.4539610000
C	-5.4020110000	-2.1894450000	0.5575530000
F	-3.9587010000	-3.0026660000	-2.6581500000
F	-6.3507630000	-4.2394350000	-2.8762210000
F	-8.1360480000	-4.1279990000	-0.8212650000
F	-7.5113610000	-2.7741980000	1.4583470000
F	-5.1224690000	-1.5343570000	1.6847530000
F	2.9081570000	-4.4107970000	-2.0439510000
F	4.1042660000	-6.8062390000	-1.6749590000
F	3.9751940000	-8.0347670000	0.7542520000
F	2.6358730000	-6.8559580000	2.8113260000
F	1.4320770000	-4.4626110000	2.4477070000
N	0.5448010000	1.9070780000	-0.2698090000
C	1.8433070000	2.3587730000	-0.3603620000
C	1.8798670000	3.8008050000	-0.3035440000
C	0.5955470000	4.2194510000	-0.1360470000
C	-0.2320440000	3.0356420000	-0.1302340000
C	2.9820750000	1.5592630000	-0.4380170000

C	4.3143990000	2.2258080000	-0.4898800000
C	4.8449640000	2.8594000000	0.6384090000
C	6.0917130000	3.4824400000	0.6106040000
C	6.8387410000	3.4718700000	-0.5680020000
C	6.3368040000	2.8402370000	-1.7062470000
C	5.0859300000	2.2262220000	-1.6551900000
C	-1.6253050000	3.0647390000	-0.0579450000
C	-2.3074410000	4.3818060000	0.0891520000
C	-2.3192120000	5.3249620000	-0.9435670000
C	-2.9648530000	6.5533520000	-0.8095370000
C	-3.6245590000	6.8570240000	0.3816080000
C	-3.6334800000	5.9337740000	1.4274370000
C	-2.9794740000	4.7125070000	1.2708970000
F	-1.7014450000	5.0601420000	-2.0962890000
F	-2.9596660000	7.4329540000	-1.8089540000
F	-4.2437500000	8.0242180000	0.5197320000
F	-4.2622230000	6.2238730000	2.5642420000
F	-3.0080830000	3.8471420000	2.2845470000
F	4.1518620000	2.8776800000	1.7775430000
F	6.5742440000	4.0810990000	1.6973120000
F	8.0284140000	4.0620220000	-0.6057000000
F	7.0512450000	2.8296700000	-2.8296200000
F	4.6310810000	1.6219450000	-2.7539830000
N	-1.9769270000	0.6251760000	-0.2299910000
C	-3.1095480000	-0.1522310000	-0.3435450000
C	-4.2875130000	0.6812180000	-0.3886170000
C	-3.8640220000	1.9680830000	-0.2531440000
C	-2.4242490000	1.9250020000	-0.1547390000
N	1.8150280000	-0.6118350000	-0.2819970000
C	2.9483980000	0.1663100000	-0.3832710000

C	4.1313980000	-0.6579010000	-0.3307360000
C	3.7086540000	-1.9412200000	-0.1633890000
C	2.2663910000	-1.9069050000	-0.1373630000
O	1.2647350000	0.9006850000	2.3561460000
N	2.1917490000	0.1906580000	2.8187990000
O	2.1976400000	-1.0015590000	2.7628670000
H	0.2359750000	5.2400120000	-0.0346930000
H	2.7759170000	4.4115590000	-0.3760330000
H	-2.9375740000	-4.3928160000	-0.2064430000
H	-0.3826130000	-5.2202720000	0.0445620000
H	-5.3065580000	0.3244990000	-0.5131700000
H	-4.4667490000	2.8725850000	-0.2465860000
H	4.3196990000	-2.8337440000	-0.0590010000
H	5.1541170000	-0.2950820000	-0.3896910000

TS2

C	-1.5041060000	2.6199500000	-0.3414070000
N	-0.2850970000	1.9870550000	-0.1774640000
C	0.6413620000	2.9945270000	0.0229320000
C	-0.0119620000	4.2746770000	-0.0058470000
C	-1.3320260000	4.0448300000	-0.2674710000
Fe	0.0619370000	0.0218980000	-0.2379820000
N	2.0163070000	0.3613830000	-0.1461880000
C	2.6407050000	1.5806860000	0.0579200000
C	4.0671410000	1.4080130000	0.0581900000
C	4.3105850000	0.0837010000	-0.1665230000
C	3.0344700000	-0.5657920000	-0.2799690000
C	2.0149390000	2.8212220000	0.1798360000
C	2.8640950000	4.0178270000	0.4421620000

C	3.4462860000	4.2176230000	1.6983710000
C	4.2475230000	5.3262090000	1.9669260000
C	4.4824800000	6.2630190000	0.9596580000
C	3.9177960000	6.0864000000	-0.3042770000
C	3.1201750000	4.9695750000	-0.5498540000
C	2.8768980000	-1.9422830000	-0.4330130000
C	4.1003520000	-2.7761830000	-0.6065000000
C	4.8200320000	-2.7544670000	-1.8055980000
C	5.9747580000	-3.5153450000	-1.9816840000
C	6.4320890000	-4.3206830000	-0.9380400000
C	5.7351450000	-4.3591960000	0.2703410000
C	4.5845520000	-3.5873420000	0.4246870000
F	4.4065750000	-1.9870000000	-2.8149060000
F	6.6396210000	-3.4778430000	-3.1330820000
F	7.5302620000	-5.0489930000	-1.0940760000
F	6.1737480000	-5.1239700000	1.2662500000
F	3.9400200000	-3.6360120000	1.5910230000
F	3.2393100000	3.3321860000	2.6736560000
F	4.7857510000	5.4956340000	3.1713080000
F	5.2423180000	7.3230280000	1.2040860000
F	4.1466010000	6.9779480000	-1.2644190000
F	2.5927330000	4.8207320000	-1.7657800000
C	-2.7401980000	1.9904710000	-0.4770470000
C	-3.9568290000	2.8284720000	-0.6736600000
C	-4.5955910000	2.8803680000	-1.9164680000
C	-5.7379260000	3.6528440000	-2.1206700000
C	-6.2658310000	4.3907540000	-1.0603130000
C	-5.6506840000	4.3531330000	0.1919060000
C	-4.5076240000	3.5753340000	0.3721510000
F	-4.1122470000	2.1769970000	-2.9411050000

F	-6.3257880000	3.6885970000	-3.3132380000
F	-7.3538930000	5.1280390000	-1.2432040000
F	-6.1570460000	5.0547650000	1.2020530000
F	-3.9332540000	3.5580420000	1.5753560000
N	-1.8900470000	-0.3237560000	-0.2201310000
C	-2.5255960000	-1.5470530000	-0.0867570000
C	-3.9498240000	-1.3704290000	-0.1390950000
C	-4.1810500000	-0.0387180000	-0.3347140000
C	-2.9013670000	0.6109750000	-0.3708690000
C	-1.9000480000	-2.7860050000	0.0395410000
C	-0.5211910000	-2.9521390000	-0.0739280000
N	0.4100520000	-1.9376910000	-0.2118550000
C	1.6339230000	-2.5689830000	-0.3625050000
C	1.4575470000	-3.9952990000	-0.3409460000
C	0.1313000000	-4.2312950000	-0.1223250000
C	-2.7549170000	-3.9797570000	0.2888630000
C	-3.3448020000	-4.1678860000	1.5430120000
C	-4.1557020000	-5.2686960000	1.8131520000
C	-4.3914080000	-6.2082600000	0.8080150000
C	-3.8158790000	-6.0441690000	-0.4527360000
C	-3.0084820000	-4.9345860000	-0.6997110000
F	-3.1344370000	-3.2758760000	2.5141480000
F	-2.4701220000	-4.7955570000	-1.9118440000
F	-4.0437680000	-6.9402810000	-1.4086440000
F	-5.1616510000	-7.2607890000	1.0522540000
F	-4.7029930000	-5.4292200000	3.0143470000
O	-0.3691680000	-0.8452470000	2.4059100000
N	-1.4259190000	-0.7494100000	2.9571730000
O	-2.4154330000	-0.1284870000	2.7553130000
H	-2.1253710000	4.7793810000	-0.3808440000

H	0.4761780000	5.2339490000	0.1440870000
H	-0.3619390000	-5.1938880000	-0.0189630000
H	2.2505550000	-4.7290150000	-0.4597880000
H	-4.6830940000	-2.1684670000	-0.0568510000
H	-5.1384190000	0.4662620000	-0.4305620000
H	5.2744710000	-0.4140320000	-0.2298340000
H	4.7946980000	2.2031530000	0.1977000000

References

1. A. D. Adler, F. R. Longo, J. D. Finarelli, J. Goldmacher, J. Assour and L. Korsakoff, A simplified synthesis for meso-tetraphenylporphine, *J. Org. Chem.*, 1967, **32**, 476-476.
2. M. Y. Hyun, Y. D. Jo, J. H. Lee, H. G. Lee, H. M. Park, I. H. Hwang, K. B. Kim, S. J. Lee and C. Kim, Remarkable Solvent, Porphyrin Ligand, and Substrate Effects on Participation of Multiple Active Oxidants in Manganese(III) Porphyrin Catalyzed Oxidation Reactions, *Chem. Eur. J.*, 2013, **19**, 1810-1818.
3. M. K. Peters, F. Röhricht, C. Näther and R. Herges, One-Pot Approach to Chlorins, Isobacteriochlorins, Bacteriochlorins, and Pyrrocorphins, *Org. Lett.*, 2018, **20**, 7879-7883.
4. A. Z. Muresan, P. Thamyongkit, J. R. Diers, D. Holten, J. S. Lindsey and D. F. Bocian, Regiospecifically α-13C-Labeled Porphyrins for Studies of Ground-State Hole Transfer in Multiporphyrin Arrays, *J. Org. Chem.*, 2008, **73**, 6947-6959.
5. R. A. Ghiladi, R. M. Kretzer, I. Guzei, A. L. Rheingold, Y.-M. Neuhold, K. R. Hatwell, A. D. Zuberbühler and K. D. Karlin, $(F_8TPP)Fe^{II}/O_2$ Reactivity Studies {F_8TPP = Tetrakis(2,6-difluorophenyl)porphyrinate(2−)}: Spectroscopic (UV−Visible and NMR) and Kinetic Study of Solvent-Dependent (Fe/O_2 = 1:1 or 2:1) Reversible O_2-Reduction and Ferryl Formation, *Inorg. Chem.*, 2001, **40**, 5754-5767.
6. J. Wang, M. P. Schopfer, S. C. Puiu, A. A. N. Sarjeant and K. D. Karlin, Reductive Coupling of Nitrogen Monoxide (•NO) Facilitated by Heme/Copper Complexes, *Inorg. Chem.*, 2010, **49**, 1404-1419.
7. P. Mondal, S. Rajapakse and G. B. Wijeratne, Following Nature's Footprint: Mimicking the High-Valent Heme-Oxo Mediated Indole Monooxygenation Reaction Landscape of Heme Enzymes, *J. Am. Chem. Soc.*, 2022, **144**, 3843-3854.
8. P. Mondal and G. B. Wijeratne, Modeling Tryptophan/Indoleamine 2,3-Dioxygenase with Heme Superoxide Mimics: Is Ferryl the Key Intermediate?, *J. Am. Chem. Soc.*, 2020, **142**, 1846-1856.
9. P. Mondal, I. Ishigami, E. F. Gérard, C. Lim, S.-R. Yeh, S. P. de Visser and G. B. Wijeratne, Proton-coupled electron transfer reactivities of electronically divergent heme superoxide intermediates: a kinetic, thermodynamic, and theoretical study, *Chem. Sci.*, 2021, **12**, 8872-8883.
10. P. Mondal, I. Ishigami, S.-R. Yeh and G. B. Wijeratne, The Role of Heme Peroxo Oxidants in the Rational Mechanistic Modeling of Nitric Oxide Synthase: Characterization of Key Intermediates and Elucidation of the Mechanism, *Angew. Chem. Int. Ed.*, 2022, **61**, e202211521.
11. M. Selke, M. F. Sisemore and J. S. Valentine, The Diverse Reactivity of Peroxy Ferric Porphyrin Complexes of Electron-Rich and Electron-Poor Porphyrins, *J. Am. Chem. Soc.*, 1996, **118**, 2008-2012.
12. S. B. Jayawardana, P. Mondal, C. B. Gabel, G. Olajide, D. A. Decato, N. C. Suffern, T. Szilvasi, B. S. Pierce, P. Moënne-Loccoz and G. B. Wijeratne, From Transient to Metastable: Generation, Characterization, and Biomimetic Reactivity Studies of Well-Defined Heme Peroxynitrite Model Systems, *J. Am. Chem. Soc.*, 2025, **147**, 41524-41538.

13. P. Mondal, D. Udukalage, A. A. Mohamed, H. P. H. Wong, S. P. de Visser and G. B. Wijeratne, A Cytochrome P450 TxtE Model System with Mechanistic and Theoretical Evidence for a Heme Peroxynitrite Active Species, *Angew. Chem. Int. Ed.*, 2024, **136**, e202409430.

14. L. C. Green, D. A. Wagner, J. Glogowski, P. L. Skipper, J. S. Wishnok and S. R. Tannenbaum, Analysis of nitrate, nitrite, and [15N]nitrate in biological fluids, *Anal. Biochem.*, 1982, **126**, 131-138.

15. P. Kumar, Y.-M. Lee, Y. J. Park, M. A. Siegler, K. D. Karlin and W. Nam, Reactions of Co(III)–Nitrosyl Complexes with Superoxide and Their Mechanistic Insights, *J. Am. Chem. Soc.*, 2015, **137**, 4284-4287.

16. J. Su and J. T. Groves, Mechanisms of Peroxynitrite Interactions with Heme Proteins, *Inorg. Chem.*, 2010, **49**, 6317-6329.

17. G. B. Wijeratne, M. Bhadra, M. A. Siegler and K. D. Karlin, Copper(I) Complex Mediated Nitric Oxide Reductive Coupling: Ligand Hydrogen Bonding Derived Proton Transfer Promotes N2O(g) Release, *J. Am. Chem. Soc.*, 2019, **141**, 17962-17967.

18. M. J. T. Frisch, G. W.; Schlegel, H. B.; Scuseria, G. E.; Robb, M. A.; Cheeseman, J. R.; Scalmani, G.; Barone, V.; Petersson, G. A.; Nakatsuji, H.; Li, X.; Caricato, M.; Marenich, A. V.; Bloino, J.; Janesko, B. G.; Gomperts, R.; Mennucci, B.; Hratchian, H. P.; Ortiz, J. V.; Izmaylov, A. F.; Sonnenberg, J. L.; Williams; Ding, F.; Lipparini, F.; Egidi, F.; Goings, J.; Peng, B.; Petrone, A.; Henderson, T.; Ranasinghe, D.; Zakrzewski, V. G.; Gao, J.; Rega, N.; Zheng, G.; Liang, W.; Hada, M.; Ehara, M.; Toyota, K.; Fukuda, R.; Hasegawa, J.; Ishida, M.; Nakajima, T.; Honda, Y.; Kitao, O.; Nakai, H.; Vreven, T.; Throssell, K.; Montgomery Jr., J. A.; Peralta, J. E.; Ogliaro, F.; Bearpark, M. J.; Heyd, J. J.; Brothers, E. N.; Kudin, K. N.; Staroverov, V. N.; Keith, T. A.; Kobayashi, R.; Normand, J.; Raghavachari, K.; Rendell, A. P.; Burant, J. C.; Iyengar, S. S.; Tomasi, J.; Cossi, M.; Millam, J. M.; Klene, M.; Adamo, C.; Cammi, R.; Ochterski, J. W.; Martin, R. L.; Morokuma, K.; Farkas, O.; Foresman, J. B.; Fox, D. J., Gaussian 16 Rev. C.01, *Wallingford, CT,*, 2016.

19. F. Weigend and R. Ahlrichs, Balanced basis sets of split valence, triple zeta valence and quadruple zeta valence quality for H to Rn: Design and assessment of accuracy, *Phys. Chem. Chem. Phys.*, 2005, **7**, 3297-3305.

20. A. V. Marenich, C. J. Cramer and D. G. Truhlar, Universal solvation model based on solute electron density and on a continuum model of the solvent defined by the bulk dielectric constant and atomic surface tensions, *J. Phys. Chem. B*, 2009, **113**, 6378-6396.

21. A. Becke, Density-functional thermochemistry. III. The role of exact exchange (1993) *J, Chem. Phys.*, **98**, 5648.

22. S. Grimme, J. Antony, S. Ehrlich and H. Krieg, A consistent and accurate ab initio parametrization of density functional dispersion correction (DFT-D) for the 94 elements H-Pu, *J, Chem. Phys.*, 2010, **132**.

23. S. Grimme, S. Ehrlich and L. Goerigk, Effect of the damping function in dispersion corrected density functional theory, *J. Comput. Chem.*, 2011, **32**, 1456-1465.

24. C. Lee, W. Yang and R. G. Parr, Development of the Colle-Salvetti correlation-energy formula into a functional of the electron density, *Phys. Rev. B*, 1988, **37**, 785.

25. G. Luchini, J. V. Alegre-Requena, I. Funes-Ardoiz and R. S. Paton, GoodVibes: automated thermochemistry for heterogeneous computational chemistry data, *F1000Res.*, 2020, **9**, 291.

26. D. T. Petasis and M. P. Hendrich, in *Methods in Enzymology*, eds. P. Z. Qin and K. Warncke, Academic Press, 2015, vol. 563, pp. 171-208.

27. A. P. Golombek and M. P. Hendrich, Quantitative analysis of dinuclear manganese(II) EPR spectra, *J Magn Reson*, 2003, **165**, 33-48.

28. A. Bencini and D. Gatteschi, *Electron Paramagnetic Resonance of Exchange Coupled Systems*, Springer-Verlag, 1990.

29. J. A. Weil, J. R. Bolton and J. E. Wertz, *Electron Paramagnetic Resonance: Elementary Theory and Practial Applications*, John Wiley & Sons, Inc., New York.

30. A. Abragam and B. Bleaney, *Electron Paramagnetic Resonance of Transition Ions (International Series of Monographs on Physics)*, 1970.

31. C. D. Cohen-Tannoudji, B.; Dui, B.; Laloë, F.; Hemley, S. R.; Ostrowsky, N.; Ostrowsky, D. B., *Quantum Mechanics*, Wiley, 1977.

32. S. Rajapakse, Y. Lee, S. B. Jayawardana, J. Helms, P. Mondal, A. Singh, B. S. Pierce, H. S. Shafaat and G. B. Wijeratne, Modulation of heme peroxo nucleophilicities with axial ligands reveal key insights into the mechanistic landscape of nitric oxide synthase, *Chem. Sci.*, 2025, **16**, 9648-9661.

33. V. S. Oganesyan and Y. A. Sharonov, Determination of zero-field splitting and evidence for the presence of charge-transfer transitions in the Soret region of high-spin ferric hemoproteins obtained from an analysis of low-temperature magnetic circular dichroism, *Biochim Biophys Acta.*, 1998, **1429**, 163-175.

34. G. Palmer, *The Porphyrins-Chapter 6 Electron Paramagnetic Resonance of Hemoproteins*, Academic Press, 1978.

35. M. Weissbluth, Berlin, Heidelberg, 1967.

36. I. García-Rubio, M. Braun, I. Gromov, L. Thöny-Meyer and A. Schweiger, Axial Coordination of Heme in Ferric CcmE Chaperone Characterized by EPR Spectroscopy, *Biophys J.*, 2007, **92**, 1361-1373.

37. J. Nehrkorn, B. M. Martins, K. Holldack, S. Stoll, H. Dobbek, R. Bittl and A. Schnegg, Zero-field splittings in metHb and metMb with aquo and fluoro ligands: a FD-FT THz-EPR study, *Mol. Phys.*, 2013, **111**, 2696-2707.

38. J. Peisach and W. E. Blumberg, Structural implications derived from the analysis of electron paramagnetic resonance spectra of natural and artificial copper proteins, *Arch Biochem Biophys*, 1974, **165**, 691-708.